Local Structure of Hydrogen-Bonded Liquids

by

Matteo Cavalleri

Stockholm University 2004

Dissertation for the Degree of Doctor of Philosophy in Chemical Physics presented at Stockholm University in 2004

Abstract

Ordinary yet unique, water is the substance on which life is based. Water seems, at first sight, to be a very simple molecule, consisting of two hydrogen atoms attached to one oxygen. Its small size belies the complexity of its action and its numerous anomalies, central to a broad class of important phenomena, ranging from global current circulation, terrestrial water and CO_2 cycles to corrosion and wetting. The explanation of this complex behavior comes from water's unique ability to form extensive three-dimensional networks of hydrogen–bonds, whose nature and structures, in spite of a great deal of efforts involving a plethora of experimental and theoretical techniques, still lacks a complete scientific understanding.

This thesis is devoted to the study of the local structure of hydrogen–bonded liquids, with a particular emphasis on water, taking advantage of a combination of core–level spectroscopies and density functional theory spectra calculations. X–ray absorption, in particular, is found to be sensitive to the local hydrogen–bond environment, thus offering a very promising tool for spectroscopic identification of specific structural configurations in water, alcohols and aqueous solutions. More specifically, the characteristic spectroscopic signature of the broken hydrogen–bond at the hydrogen side is used to analyze the structure of bulk water, leading to the finding that most molecules are arranged in two hydrogen–bond configurations, in contrast to the picture provided by molecular dynamics simulations. At the liquid–vapor interface, an interplay of surface sensitive measurements and theoretical calculations enables us to distinguish a new interfacial species in equilibrium with the gas. In a similar approach the cluster form of the excess proton in highly concentrated acid solutions and the different coordination of methanol at the vacuum interface and in the bulk can also be clearly identified.

Finally the ability of core–level spectroscopies, aided by sophisticated density functional theory calculations, to directly probe the valence electronic structure of a system is used to observe the nature of the interaction between water molecules and solvated ions in solution. Water around transition metal ions is found to interact with the solute via orbital mixing with the metal d–orbitals. The hydrogen–bond between water molecules is explained in terms of electrostatic interactions enhanced by charge rehybridization in which charge transfer between connecting molecules is shown to be fundamental.

Matteo Cavalleri
Department of Physics
Stockholm University
AlbaNova University Center
SE-106 91 Stockholm
Sweden

ISBN 91–7265–969–6 pp. 1–66.

Printed in Sweden by Universitetsservice US–AB, Stockholm (2004)

List of papers

This thesis is based on the following papers which will be referred to in the text by their roman numerals. Reprints were made with kind permission from the publishers.

I. Spectroscopic probing of local hydrogen–bonding structures in liquid water
S. Myneni, Y. Luo, L.Å. Näslund, M. Cavalleri, L. Ojamäe, H. Ogasawara, A. Pelmenschikov, P. Väterlein, C. Heske, L.G.M. Pettersson and A. Nilsson
J. Phys. Cond. Matt. **14**, *L213*, 2002

II. Characterization of hydrogen bond acceptor molecules at the water surface using near–edge x–ray absorption fine–structure spectroscopy and density functional theory
K.R. Wilson, M. Cavalleri, B. S Rude, R. D. Schaller, A. Nilsson, L.G.M. Pettersson, N. Goldman, T. Catalano, J.D. Bozek and R.J. Saykally
J. Phys. Cond. Matt. **14**, *L221*, 2002

III. The structure of the first coordination shell in liquid water
Ph. Wernet, D. Nordlund, U. Bergmann, M. Cavalleri, M. Odelius, H. Ogasawara, L.Å. Näslund, T.K. Hirsch, L. Ojamäe, P. Glatzel, L.G.M. Pettersson and A. Nilsson
Science **304**, *995*, 2004 published online 01 April 04, 10.1126/science.1096205

IV. Modeling the x–ray absorption spectrum of liquid water by molecular dynamics simulations
M. Odelius, M. Cavalleri, A. Nilsson and L.G.M. Pettersson
In manuscript

V. Half and full core–hole approximations in computed x–ray absorption spectra of water
M. Cavalleri, D. Nordlund, M. Odelius, A. Nilsson and L.G.M. Pettersson
Submitted to *J. Chem. Phys.*

VI. X–ray absorption spectra of water within a plane–wave Car–Parrinello molecular dynamics framework
M. Cavalleri, M. Odelius, A. Nilsson and L.G.M. Pettersson
J. Chem. Phys. **121**, *Issue 19*, 2004

VII. X–ray absorption signature of protonated clusters in acid solution
M. Cavalleri, L.Å. Näslund, D.C. Edwards, Ph. Wernet, H. Ogasawara, S. Myneni, L. Ojamäe, A. Nilsson and L.G.M. Pettersson
In manuscript

VIII. X–ray absorption spectroscopy of liquid methanol microjets: surface vs. bulk electronic structure and hydrogen bonding
K.R. Wilson, M. Cavalleri, B. S Rude, R. D. Schaller, T. Catalano, A. Nilsson, L.G.M. Pettersson and R.J. Saykally
Accepted for publication in *J. Phys. Chem. B*

IX. Direct evidence of orbital mixing between water and solvated transition-metal ions: An oxygen 1s XAS and DFT study of aqueous systems
L.Å. Näslund, M. Cavalleri, H. Ogasawara, A. Nilsson, L.G.M. Pettersson, Ph. Wernet, D.C. Edwards, M. Sandström and S. Myneni
J. Phys. Chem. A **107**, *6869*, 2003

X. The interpretation of X–ray absorption spectra of water and ice
M. Cavalleri, H. Ogasawara, L.G.M. Pettersson and A. Nilsson
Chem. Phys. Lett. **364**, *363*, 2002

XI. The hydrogen bond in ice probed by soft x–ray spectroscopy and density functional theory
A. Nilsson, H. Ogasawara, M. Cavalleri, D. Nordlund, M. Nyberg, Ph. Wernet and L.G.M. Pettersson
Submitted to *J. Chem. Phys.*

Related papers to which I have contributed but which are not included in this thesis:

- **X–ray Raman spectroscopy at the oxygen K edge of water and ice: Implications on local structure models**
U. Bergmann, Ph. Wernet, P. Glatzel, M. Cavalleri, L.G.M. Pettersson, A. Nilsson and S.P. Cramer
Phys. Rev. B **66**, *092107*, 2002

- **Electronic structure effects from hydrogen bonding in the liquid phase and in chemisorption: an integrated theory and experimental effort**
L.G.M. Pettersson, A. Nilsson, S. Myneni, Y. Luo, M. Nyberg, M. Cavalleri, L. Ojamäe, L.Å. Näslund, H. Ogasawara, M. Odelius, A.G. Pelmenschikov
J. Synch. Rad. **140**, *131*, 2001

Contents

There is a theory which states that if ever anybody discovers exactly what the Universe is for and why it is here, it will instantly disappear and be replaced by something even more bizarre and inexplicable... There is another theory which states that this has already happened.

Douglas Adams, *The Restaurant at the End of the Universe*

Chapter 1

Introduction

Water is the chemical substance with which we are most familiar; it covers 70% of the surface of the earth and accounts for 55-65% of our body weight, it is found in our solar system and even in outer space in comet nuclei and cosmic dust. If a non-scientist knows only one chemical formula it is a fair bet to say that this is H_2O.

Although water is the most common, most ubiquitous of all liquids it is also the most unusual. To start with, it's a liquid under the conditions we live in and it should not be. Similar small molecules like methane and hydrogen sulphide, SH_2, which has the same kinked shape as water (we will come to the shape of the water molecule in section 2.2), boil well below O °C while water has exceptionally high melting and boiling points.

Furthermore water freezes "top-down", causing for example lakes and rivers to grow an ice layer during winter on top of water a few degrees warmer. Usually substances freeze "bottom-up" because they become more dense when solidified and therefore sink to the bottom of their liquid. This anomaly has fundamental implications far beyond simply allowing us to skate over frozen lakes during the Swedish winter; if the polar seas would freeze from below, the ocean circulation could not take place since it involves mainly bottom waters, and the northern regions would be much colder than what they already are. The reason for this is that water has its maximum density not at its freezing point but slightly above, at 4 °C, a behavior which is unexpected by the general law of expansion.

Many other oddities of water have implications of global significance; its large heat capacity is responsible for the thermal stability of a living body and allows for example warm ocean currents to carry phenomenal amounts of heat (that's why, thanks to the Gulf Stream, northern Europe is much warmer than the Canadian coasts at the same latitude) and the high surface tension allows water from the roots to reach trees' higher leaves. While most liquids increase their viscosity under pressure, water flows faster when squeezed.

Although water isn't alone in displaying any one of these anomalies, it is their combination in a single substance that makes it stand out as the most unusual, yet the most important, of the liquids. Most of the oddities of water have their origin in the peculiar intermolecular attractive force between neighboring molecules: the

hydrogen bond (HB) [1].

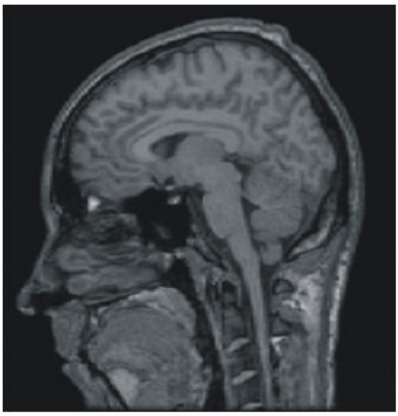

Figure 1.1: The brain of the author. Water accounts for 70% of its weight. T1-weighted anatomical MRI image in the sagittal (medial-lateral) plane taken by Christina Schmitz at Karolinska Sjukhuset, Stockholm.

Generally speaking, a hydrogen bond is the attractive force between the hydrogen attached to an electronegative atom of one molecule and the electronegative atom of a neighboring molecule. Usually the electronegative atom is oxygen, nitrogen, or fluorine, which all have a partial negative charge. The hydrogen then has the partial positive charge. This attraction is about ten times stronger than the van der Waals forces that are responsible for holding "normal" liquids together but also ten times weaker than the intramolecular covalent bond between O and H in the water molecule. The hydrogen bond in water is anyway sufficiently strong to guarantee the extra cohesion that prevents vaporization and sufficiently directional to impose structural constraints on the positions and orientations of neighboring molecules, which in turn affect physical properties like density, heat capacity and viscosity. In this respect water is more like a crystal than a liquid; it is more highly structured and it is attractive forces instead of repulsive, like in "normal liquids", that are responsible for the way the molecules are packed in the condensed phase.

The hydrogen bond not only affects the structure and the properties of liquid water (papers I to VI deal with the hydrogen bonding network in liquid water) but as well the way water accommodates dissolved ions (targeted in papers VII and IX).

The capacity for making hydrogen bonds is not exclusive to water but only water has the right shape to allow the formation of up to four (and even, rarely, five) HBs and extend the network throughout the directions in space. The uncanny flexibility as well as strength of the hydrogen bond in water is manifest in its

[1] Simpler explanations are anyway available; for example in the words of the good Reverend Dr. Brewer in his "Guide to the Scientific Knowledge of Things Familiar" (1879):
Q: When does water begin to expand from cold?
A: When it is reduced to 40 degrees (Fahrenheit, 4 °C). It is wisely ordained by God that water shall be an exception to a very general rule, it contracts till it is reduced to 40 degrees, and then it expands till it freezes.

thirteen different crystalline forms confirmed thus far.

With only one hydrogen atom bound to the oxygen, alcohols for example can donate and accept only one hydrogen bond and therefore molecules are linked into two–dimensional chains or rings (paper VIII) rather than in more complex three–dimensional networks.

How to Read This Thesis

This thesis has been written with the idea in mind that each of its sections should be self-containing and, as such, able to be read independently from each other. Considering the endless number of inter–crossing references in the text I now assume I failed in this task.

However, the reader who has picked up this thesis interested in a short overview of the present knowledge over the hydrogen–bonding interaction and the most common hydrogen–bonded systems should be satisfied with having a look only at Chapter 2.

Chapter 3 quickly sets up the theoretical framework of the spectra calculations and the density functional theory upon which they are based and introduces the most important aspects of the core–level spectroscopies used throughout this research project. Those familiar with these subjects can easily skip this section.

Finally, in Chapter 4 I provide a brief summary of the main results of the articles on which this thesis is based.

Those of you who have received this thesis as a sign of my gratitude for the wonderful times together and don't really care about it can go directly to the crossworld puzzle at the end of this book; it is meant to help you through the three hours of the dissertation. Thank you for being there, by the way.

Chapter 2

Water and the Hydrogen Bond

The ubiquity of water in nature is reflected in its ubiquity in the scientific literature. The relevance that water has for life had not escaped the attention of men[1] since antiquity and research into the nature and the properties of this fascinating liquid has been conducted continuously throughout history to reach the actual pace of almost one paper per day published on the subject. In this light it can be seen as very surprising that there is any need at all for, if not this thesis, any further investigation at all. Still, new experimental techniques and new theoretical tools, like those introduced in this thesis, are required to account for the fast dynamics and the complexity of the hydrogen–bond in water.

This chapter is intended to offer a quick up–to–date overview of the hydrogen–bonded systems that are the object of investigation in this thesis and of the clues they have offered to lead scientists to the current understanding of their structure and properties. But we start with a bit of history first.

2.1 Brief History of Water Research

Water has been regarded as a fundamental substance for life and the composition of matter since antiquity [1]. For the Greek philosopher Thales of Ionia (6th century B.C.) water represented the single elemental substance from which it was possible to derive all matter. He based his model on the observation that water was the only substance known to be able to transform itself into both a gas and a solid. Since Thales, water has always been part of the esteemed family of fundamental substances used by philosophers to explain the universe they observed. In the Aristotelian model, which heavily influenced the scientific knowledge until the end of the medieval period, water was joined by earth, air and fire while ancient Chinese tradition (attributed to scholar Tsou Yen, who lived around 350 B.C.) had 5 elements: earth, metal, wood, fire and of course water.

[1] and women, of course.

In the early stage of the Renaissance, Leonardo da Vinci was the first one to study the dynamics of water with a rigorous scientific approach [2]. The history of modern water research begins in 1783 when Antoine Laurent Lavoisier perfected the earlier experiments of Cavendish and Priestley and confirmed that water is composed of oxygen and hydrogen burying for good the ancient idea of "elementary water" [3]. Dalton's first guess at the chemical formula for water, a binary molecule consisting of one oxygen and one hydrogen atom was later corrected in 1826 by the Swedish chemist Jöns Jakob Berzelius who made it clear that water must contain two hydrogen atoms and one oxygen. Berzelius began denoting chemical substances by sequences of the respective element symbols, derived from the Latin forms of their name, with superscripts indicating the number of each atom in the molecule if there was more than one. So water became H^2O, to assume the well-known H_2O denomination later in the 19th century when superscripts were rendered as subscripts.

By 1930 most of the unusual properties of water seemed to be known but, except for thermodynamical observations, very little experimental data on water were available. The 1930s represent a golden age for water research; the first x–ray diffraction data on liquid water were independently published by Meyer [4] in 1930 and Stewart [5] and Amaldi [6] in 1931, the spectroscopic proof of the V–shaped geometry of the water molecule [7] came in 1932 and as early as 1933 Bernal and Fowler proposed the first realistic interaction potential for water, based on simple electrostatic considerations in addition to a repulsion–dispersion term [8]. In 1935 Linus Pauling, the most influential chemist of the century, introduced for the first time the term "hydrogen bond" to account for the residual entropy of Ice [9].

The first computer simulation of liquid water came in the late 1960s by Barker and Watts [10] and Rahman and Stillinger [11] and, since then, theoretical modeling has played an increasing role in the interpretation of experimental data of water, alcohols and other hydrogen-bonded liquids. From those early times an impressive number of interaction potentials for simulations have been and still are introduced in the literature [12], with the milestone of the first *ab initio* molecular dynamics of liquid water in 1993 [13].

2.2 The Water Molecule

The water molecule consists of two hydrogen atoms bonded through a rather strong covalent interaction to an oxygen atom. H_2O has a planar V–shape structure (C_{2v} symmetry) characterized by an H-O-H angle of 104.5° and O–H bond length of 0.957 Å (5.2 eV is needed to break the intramolecular O–H bond).

The molecular orbitals (MOs) of H_2O are shown in figure 2.1. The atomic oxygen p- and hydrogen s–orbitals mix, causing the sp^3 hybridization of the MOs which in turn is the origin of the tetrahedral distribution of the electrons around the oxygen atom. Such a shape makes water ideally suited to both accept and donate two hydrogens and thus form complex three–dimensional hydrogen–bonding networks upon condensation.

In the molecule most of the electron density is centered on the electronegative oxygen atom and, in particular, the lone–pair orbitals which give a rather strong

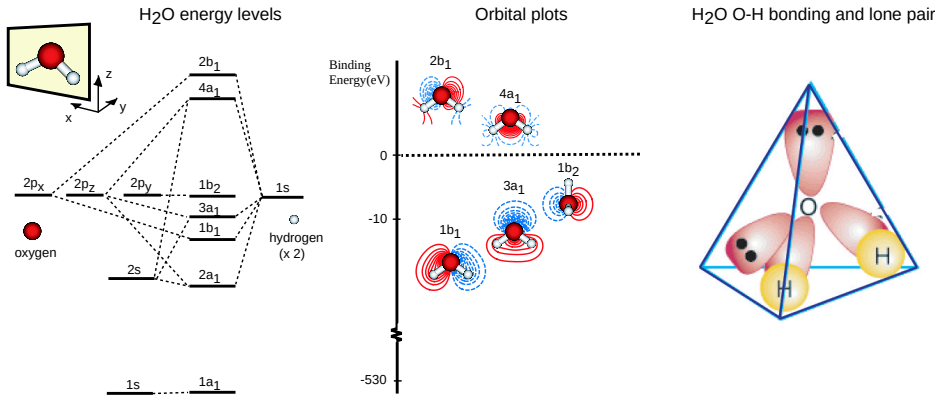

Figure 2.1: Molecular orbital energy level diagram for H_2O (left). Orbital plots of the gas phase molecule valence states. The plots are shown in the gas–phase binding energy scale (middle). The tetrahedral electron density of H_2O (right).

intramolecular dipole moment (1.855 D). This is a quite large value compared to other polar molecules such as CO (0.1 D) and NO (0.16 D) and it is responsible for making water the most important polar solvent in nature.

The interaction between water molecules is dominated by the hydrogen–bond. As briefly mentioned in this thesis' introduction, a HB is formed when the hydrogen atom of one water molecule interacts with the oxygen lone–pair in a neighboring molecule resulting in a nearly perfectly linear O–H...O bond. Energetically the HB is intermediate between covalent and van der Waals bonding [14]; in water having a strength on the order of 10 % of the intramolecular O–H bond.

Traditionally the hydrogen bond is seen as an electrostatic interaction between a positively charged hydrogen atom connected to an electronegative center and a negatively charged O, F or N atom. In reality such a simple picture is insufficient to describe the nature of the HB. An important aspect to consider is that hydrogen–bonds do not break or form independently from each other but rather act "cooperatively". The cooperativity of the hydrogen bond is manifest in the change of the HB (oxygen–oxygen) distance in water clusters of increasing size, as proved by infrared (IR) spectroscopic studies [15]. In the water dimer the O–O distance is $\sim$ 2.95 Å. In the trimer the HB length decreases substantially to $\sim$ 2.85 Å, indicating that the mere addition of another water molecule to the cluster makes the hydrogen–bond stronger. The O–O distance decreases further in the tetramer ($\sim$ 2.79 Å) to converge to the bulk ice value ($\sim$ 2.75 Å) in the pentamer. The cooperative nature of the hydrogen bond is also disclosed through theoretical studies. When the bonding energy per water molecule in HB chains of different sizes, but constant O–O distances, is computed it is found that the non–additive part of the hydrogen–bond increases up to 16% of the total energy [16]. It is clear that the electronic structure of the water molecule is also affected when hydrogen–bonds are formed. Firm evidence for this fact is offered by the observation that the dipole moment of water changes upon condensation, passing from 1.855 D of the gas phase molecule to 2.6–3.1 D in liquid water and ice [17].

Questions have been raised as to whether these changes should be attributed

to purely electrostatic factors as internal polarization from the field of surrounding molecules [18–21] or to some level of charge transfer process [22–24] taking place when the hydrogen–bond is formed. Claims for a covalent nature of the hydrogen bond have been made based on the analysis of the anisotropy in x–ray Compton scattering [25] experiments but this conclusion has been heavily disputed [26, 27].

Theoretical studies give contrasting results [18–22, 24, 28]. The case of the water dimer particularly exemplifies how the HB picture emerging through *ab initio* calculations can vary when different energy partitioning schemes are applied [18, 21, 22]. Using a natural bond orbital (NBO) analysis to eliminate the charge–transfer contribution from the Hamiltonian, Weinhold and coworkers [22] attribute to it the major part of the interaction energy while the electrostatic attraction is largely canceled by exchange repulsion. In the scheme provided by the Morokuma analysis and the self–consistent charge and configuration method for subsystems (SCCCMS), on the other hand, the charge transfer energy is found to be of negligible importance in stabilizing the HB of the water dimer [18, 21]. Unfortunately the lack of direct experimental evidence capable to validate either of these two contrasting pictures of the nature of the hydrogen–bond makes any result based on the interaction energy decomposition rather inconclusive.

In paper XI we use the constrained space orbital variation (CSOV) analysis [29,30], combined with spectroscopic measurements, to individually investigate different contributions to the total HB energy. The effects of those contributions on the electronic density of a water molecule involved in hydrogen–bonding with its neighbors are studied via the simulation of X–ray emission (XES) spectra. By comparing computed and experimental XES and photo–emission (PES) spectra of ice we are able to explain the hydrogen–bonding interaction in terms of electrostatic attraction enhanced by charge rehybridization in which charge transfer between connecting molecules is shown to be fundamental.

2.3 Ice

The versatility of the hydrogen–bond interaction in water is evident in the complexity of the phase diagram shown in figure 2.2 in which thirteen crystalline forms of ice are present. Such flexibility is made possible by the singular characteristic of the water molecule to act both as double hydrogen donor and acceptor and form up to four nearly linear hydrogen–bonds with its neighbors.

HF, for example, forms stronger hydrogen–bonds than water but because it has only one accepting and one donating site it is limited to the formation of two–dimensional zig–zag structures in its crystalline phase. Ammonia (NH_3) acting triply as hydrogen donor and triply as hydrogen acceptor seems to be a fair candidate to produce three–dimensional structures similar to those in ice. However because its geometry and size are ill–suited for the local arrangement with six neighbors required for the formation of linear hydrogen–bonds of the optimal length the hydrogen–bonds in solid NH_3 are substantially more strained and weakened compared to water. It is the unparalleled possibility of building extensive three–dimensional intramolecular networks that makes water stand out from the other hydrogen–bonded systems and present e.g. unusually higher melting point

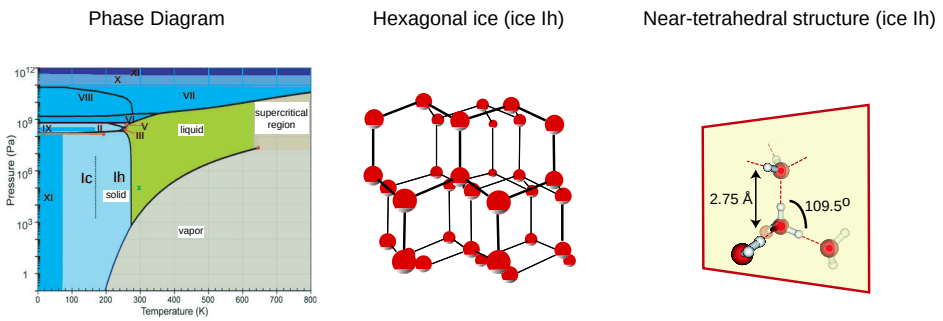

Figure 2.2: The phase diagram of water (left). The crystalline structure of hexagonal ice Ih (middle). Tetrahedral coordination of the water molecule in ice (right).

(O °C) than NH_3 (- 78 °C) and HF (- 84 °C) despite the fact that nitrogen and fluorine lie just next to oxygen in the periodic table.

The "natural" form of ice[2], the so–called hexagonal ice or phase Ih, is considered to be the model system of the H_2O HB network. In hexagonal ice each oxygen atom is placed at the vertex of a tetrahedron surrounded by 4 other oxygens at a distance of 2.75 Å. The angle between oxygen atoms is rather close to that of a geometrical tetrahedron (109.5°). According to the "ice rules", proposed by Bernal and Fowler [8], the oxygens are connected through hydrogen–bonds in such a way that only one hydrogen atom is allowed for each O–O bisectrix. Because of entropy the hydrogens are randomly distributed in the oxygen lattice leading to what is referred to as "proton disorder" in ice.

The tetrahedral local arrangement of the oxygen lattice in ice Ih is well characterized by x–ray (XRD) and neutron diffraction. XRD probes the electronic density distribution within the system. Because in H_2O, as seen in section 2.2, this is mainly centered on the oxygen atom this technique can only marginally reveal the positions of the hydrogen atoms in the crystal. Neutrons are instead scattered by the nuclei in the system. By taking advantage of the considerable difference in the coherent scattering lengths of hydrogen and deuterium it is in principle possible to extract structural information on the proton positions in the lattice from diffraction measurements of light ice, heavy ice and their mixture in various proportions. As this method is based on the unproven assumption of the structural equivalence of light and heavy ice the accuracy of the obtained intramolecular O–H distance is yet to be determined.

The bulk arrangement of four hydrogen–bonded neighbors remains the rule also for high–pressure ices; small deviations from the tetrahedral local structure via bending of the hydrogen bond directions characterize ice forms at moderate pressures (Ice II through VI and Ice IX) yet perfect local tetrahedrality is restored at the highest pressures (Ice VII and VIII) as H_2O molecules adopt an arrangement of two interpenetrating hexagonal ice networks.

The structure of the ice surface is much harder to characterize. Surface–

[2]By "natural" I mean of course the ice that forms at normal pressure and temperature conditions. This is the ice that freezes on the top of lakes, we use to cool our drinks and which falls from the sky in form of snowflakes.

sensitive topological techniques like He atomic scattering (HAS) and low–energy electron diffraction (LEED) can provide information only on the oxygen atom positions and seem to support the hypothesis of the unreconstructed surface [31,32]. Conversely Fourier Transform Infrared (FTIR) data [33,34] and recent x–ray absorption (XAS) experiments [35] are instead not consistent with an ordered surface and substantiate evidence for a reconstructed isotropical model.

Whereas a general consensus on the exact structure of the ice surface is yet to be reached, the presence of free O–H groups in dominant fractions at the surface is unquestionable as coherently manifested by many different experimental techniques. In vibrational spectroscopy the sharp peak at 3600 cm^{-1} is assigned to the free O–H stretch [36,37]. This signal is quenched upon adsorption of an hydrogen–bond acceptor like NH_3 at the ice surface [38]. The large cross–section for H^+ in photon stimulated desorption (PSD) is also unambiguously attributed to uncoordinated O–H groups [39,40] at the surface.

2.4 Liquid Water

Although the tetrahedral local arrangement of molecules in ice has been characterized in detail the structure of liquid water is still far from being understood and represents an open challenge for today's chemists and physicists. Especially the last three decades, with the advent of computer simulations, have witnessed the introduction of hundreds of different models aiming to unravel the mystery of the structure and the behavior of water; nevertheless none of these models seem able to account for all properties of the real liquid.

The extent of the changes that occur to the nearly perfectly tetrahedral structure of ice upon melting is still the subject of much debate; certainly in the liquid the HB network is a dynamical system in continuous evolution on the short time scale of the breaking and formation of the hydrogen bond (in the order of 1ps) [41].

Because the local structure of water is reflected in its macroscopic behavior and its many anomalies, thermodynamical properties [42], such as the maximum density at 4 °C, the minimum in the heat capacity at 56 °C (right in the middle of its liquid temperature range), the isothermal compressibility, the viscosity and the diffusion coefficient represent a firm set of experimental data against which any reasonable water model should be checked.

Water structure is primarily determined experimentally from XRD and neutron diffraction. The most important structural information that can be derived by diffraction data analysis are the site–site radial distribution functions (RDF) which represent the isotropically averaged distribution of intermolecular distances in the liquid. Through the analysis of the oxygen–oxygen RDF it is also possible to obtain the average number of neighbors composing the hydration shell of the water molecules. The O–O RDF from the most recent XRD experiment [43] is in reasonable agreement with that obtained by neutron diffraction [44], proving the high level of accuracy reached by the measurements. From these it is found that molecules in water have an average of 4.7 neighbors at a distribution of distances centered around the mean value of 2.75 Å [43]. It must be noted, however, that RDFs lack angular information and therefore are rather insensitive to the

distortion of the hydrogen–bonds by bending from linearity.

As discussed in section 2.3, by isotopic substitution techniques O–H and H–H RDFs can also in principle be derived from neutron diffraction data of light and heavy water, although the assumption of structural equivalence between H_2O and D_2O, which is at the base of the method, was proven wrong by both experiment [45, 46] and path–integral simulations [47, 48].

By combining measurements of the proton magnetic shielding tensor with density functional theory (DFT)[3] the distribution of HB angles, together with lengths, can be obtained [49]. The results of this study are consistent with the isotropical information obtained by diffraction and reveal a certain degree of HB distortion from linearity in liquid water with a gradual decrease of spatial correlation at high temperature.

Structural information from infra–red (IR) spectroscopy generally relies on the correlation between the O–H stretching frequency and the HB length, which has been proven to be ambiguous for liquid water [50].

In recent years molecular dynamics (MD) has emerged as the most important technique in the effort to understand the properties and the structure of water and aqueous solutions at the atomic level [12]. The capability to accurately reproduce reliable experimental RDFs is the requirement set on any computer simulation in order to be validated.

Developing a classical potential able to tackle all the subtleties of the interactions in liquid water for the simulations is not straightforward, in particular because of the need to incorporate the non–additive cooperative nature of the hydrogen–bond. Even the most sophisticated *ab initio* MDs offer a somewhat incomplete description of the water–water interaction mainly due to the neglect of long–range dispersion interactions (such as van der Waals) in the DFT framework used in the calculations of the atomic forces. Furthermore an exaggerated preference of the existing DFT functionals for straight HBs has been pointed out compared with the more shallow angular dependence obtained from MP2 and coupled–cluster *ab initio* techniques [51] which could lead to a too low occurrence in the simulations of the angular distorted structures characterized in the XAS experiments of paper III. In spite of thirty years of computer simulations of water no potential of the hundreds available in the literature is able to reproduce with acceptable accuracy all properties of water over a large temperature range [12].

X–ray absorption (XAS) and X–ray Raman scattering (XRS) at the oxygen K–edge are sensitive to distortions of the HB at the H–side of the molecules in the condensed phases of water. By comparing the experimental spectra for bulk ice (characterized by tetrahedral four HB arrangement), ice surface (where a large fraction of molecules have a free O–H group) and liquid water with the aid of computer spectra simulations we are able to demonstrate that molecules in liquid water are not predominantly four–coordinated with linear HB as they are in ice but rather in asymmetric HB conformations with only two strong and two weakened distorted HB (the complete discussion of our findings is found in papers I through

[3] We use the same theoretical approach for the simulation of the core–level spectra in this thesis. Within the quantum chemical methods DFT guarantees the best balance between accuracy and computational costs as will be discussed in section 3.2.

VI). The existence of two different kinds of O–H groups in liquid water, one "strongly" and one "weakly" hydrogen–bonded was previously suggested by the results of a femtosecond-IR study [15].

The nature of the aqueous liquid–vapor interface is equally important to characterize, since it engenders important phenomena in e.g. atmospheric chemistry, and is likewise incompletely understood. Sum frequency generation (SFG) experiments have provided proof of dangling O–H bonds that stick out from the surface [52] and evidence for surface relaxation, consistent with interfacial molecules interacting more weakly at large HB distances has come from recent extended x–ray absorption fine structure (EXAFS) measurements [53]. To date, classical simulations have not captured all these surface phenomena, presumably because the interaction force–fields were fitted to reproduce properties of the bulk phases.

The combination of XAS and electronic structure calculations, described in paper II, indicates that molecules in which both hydrogens are dangling ("acceptor only") constitute important and previously unidentified components of the water–vapor interface. Eventually this finding was corroborated by an exceedingly large–scale (sufficient to stabilize a water slab 30 Å thick) *ab initio* MD of the surface of liquid water, in which 19% of the interfacial water species were characterized as "acceptor–only" [54].

2.5 Water as Solvent

One of the most remarkable and invaluable properties of water is its ability to act as strong polar solvent, which makes it possible for strong ionic salts (such as NaCl) to be completely dissolved in it. The interaction responsible for the solvation of a charged ion in aqueous solution is typically referred to as the dipole–ion interaction; the water molecules in the first hydration shell orient their dipoles according to the charge of the solvated particle (i.e. positive protons in the direction of a negative ion, the lone–pairs of the oxygen facing positive ions).

It is generally assumed that the local reorientation of the water molecules around the dissolved ions has strong effects on the HB structure of the liquid. Some ions are considered to enhance the hydrogen–bonding network ("structure makers"), others to weaken it ("structure breakers") [55]. Very recently this school–book concept has been challenged by the results of femtosecond pump–probe spectroscopy results which show no effects on the HB in water upon dissolution of different salts [56].

Structural information on ionic solutions is obtained by x–ray, neutron diffraction and EXAFS which can determine average properties like coordination numbers of the solvation shell of ions and mean distances from the solute to the nearest water shell [57]. The reorientation time of water molecules in solution can be measured by means of nuclear magnetic resonance (NMR) [58, 59], however the technique lacks specificity and it is unable to distinguish the dynamics of the water molecules in the solvation sphere of the ion from the dynamics of "bulk" molecules [57].

Through the localization of the core–hole XAS provides the needed selectivity and is used in paper IX to locally probe the electronic structure of water in the first

solvation shell of transition metal ions, finding evidence for the existence of orbital mixing between the metal d–orbitals and the water lone–pairs. Although this mechanism, which goes beyond the simple dipole–ion interaction was anticipated by theoretical calculations [60], a direct experimental electronic structure proof was previously lacking.

Nuclear quantum effects make the characterization of the structure of the solvated proton even more difficult. The major issue at hand is related to the "core" structure of the proton, i.e. whether the proton is strongly bonded to one single water (forming H_3O^+ or Eigen form [61]) or shared between two ($H_5O_2{}^+$ or Zundel form [62]). A second issue concerns the effects of the concentration on the relative stability of these two forms of protonated clusters.

While neutron and x–ray diffraction [63], NMR [64, 65] and IR [66, 67] studies seem to indicate the predominance of H_3O^+ in acid solution, *ab initio* molecular dynamics simulations suggest a nearly equal mixture of H_3O^+ and $H_5O_2{}^+$ [68,69]. Path–integral MD, in which the quantum motion of the proton is accounted for, instead supports the picture of a "delocalized proton" with no clear distinction between the Eigen and Zundel cationic forms [70].

A more recent Monte Carlo (MC) simulation [71], based on the results of XRD, identifies the H_3O^+ as the dominant species at low pH in direct disagreement with the finding of previous diffraction experiments that predicted $H_5O_2{}^+$ as "the form" of protonated water at high acid concentration [72].

XAS is found to be able to distinguish between the two protonated clusters; in particular the Eigen form presents a characteristic spectroscopic fingerprint in the experiments which is identified with the help of simulated spectra. The conclusions of this work, described in paper VII, are consistent with the finding of the MC simulation showing an increase of the H_3O^+ fraction upon acidification of the solution.

2.6 Methanol

As in the case of water, the structure of liquid alcohols is dominated by the formation of HB networks. This is reflected by methanol, the simplest of the alcohols, having one of the highest boiling points among organic liquids (65 °C). However the presence of the methyl group produces significant differences between water and methanol, limiting the latter to the possibility of donating only one HB while retaining in principle the ability of water to accept two.

Methanol can, in any case, give rise to rather complicated two–dimensional HB arrangements and no general consensus has yet been reached concerning its structure in liquids and at interfaces.

Neutron diffraction data has been ambiguously interpreted to either support [73] or contest [74, 75] Pauling's initial hypothesis of cyclic structures [76]. Computer simulations, in particular a recent *ab initio* MD [77], support the picture of methanol molecules bonded in linear chains with up to ten members, sometimes interrupted by the presence of bifurcations, while few experimental studies point to trimer and tetramer clusters [78].

X–ray emission spectroscopy (XES) aided by DFT calculations finds liquid methanol to be a combination of six- and eight–membered chains and rings [79].

In paper VIII we applied x–ray absorption spectroscopy, combined with spectrum calculations of different HB situations, to the bulk and the surface of liquid methanol. Consistent with EXAFS [80] and MD simulations our results indicate an interfacial population of short linear chains of two to four molecules in length. In bulk methanol we found evidence for longer chains (seven to fifteen members) as well as rings.

Chapter 3

Methods

In spite of the great deal of efforts, the local structure of HB liquids remains something of an enigma. Usual experimental techniques provide average information on the properties and the macroscopic behavior of the "real" system. On the other hand, theory indeed offers a picture of the system at an atomistic level but the accuracy of the results rely on the quality of the approximations made in the chosen approach. Only rarely the connection between theory and experiment is direct and unambiguous.

One reason core–level spectroscopies are so appealing is that they yield information which is local around the excited atom and instantaneous since the core–excitation is much faster than any molecular motion. Accurate spectrum calculations allow us to verify contributions and to validate the theoretical models. The aim of this section is to present a general picture of the experimental techniques applied in this thesis and their most outstanding features which highlight their importance in the study of the local structures of hydrogen bonded systems. After this the theoretical framework of the spectrum calculations, which represents my main contribution to this combined experimental/theoretical research, is presented.

3.1 Core Level Spectroscopies

The reason why x–ray absorption (XAS) and x–ray emission (XES), among other related techniques, are collected under the name of core–level spectroscopies is that they involve the creation of a core–hole and the measurement of the transitions from and into it, as presented schematically in figure 3.1.

Due to the localized nature of the core–hole we are able to investigate the local electronic structure around a specific atom in an element–specific way. It is especially this characteristic, which makes it possible to separate the contributions of adsorbates from their substrates, that has made this family of techniques particularly useful in the study of chemi- and physisorbed molecules on surfaces [81, 82].

The application of core level spectroscopies is extended to the oxygen and carbon K–edges (1s) in hydrogen bonded liquids in this thesis. Particularly in

the case of XAS this is especially challenging to achieve because the detectors in the soft x–ray region typically require high vacuum, which is not compatible with the high vapor pressure of the liquid. The development of third–generation synchrotron light sources, improved detection techniques as well as the availability of ultra–thin windows to separate the ultra–high vacuum of the beamline from a high–pressure cell containing the sample have, however, made measurements under ambient conditions possible, allowing us to e.g. record the oxygen K–edge XAS as well as X–ray Raman scattering (XRS) data of liquid water, aqueous solutions (Papers I, III, VII, IX and X) and liquid/gas interfaces (Papers II and VIII).

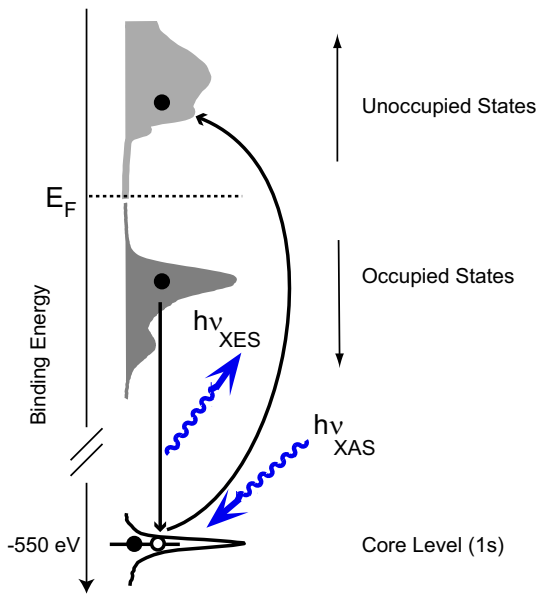

Figure 3.1: Schematic representation of the processes involved in O (1s) XAS and XES.

3.1.1 X–Ray Absorption

X–ray absorption spectroscopy [81] (XAS, sometimes also known as NEXAFS, Near Edge X–ray Absorption Fine Structure and XANES, X–ray Absorption Near Edge Structure) measures the cross–section of the transition of a core electron into the unoccupied density of states as function of the photon energy. Because the core–orbitals are localized around the nucleus of the atom, the orbitals into which the electron can be excited with largest probability are those that have large contributions close to the nucleus of the core–excited atom.

The XA transition is furthermore subjected to the dipole selection rules, so that only transitions between states whose angular momentum differs by one unit, $\Delta l = \pm 1$, will have non-zero probability; more specifically this means that in the case of K–shell excitation (we are looking at the 1s orbital) only transitions into orbitals with local p–character are allowed. In summary, XAS provides a sensitive

probe of the local, atom–projected p–type density of unoccupied states.

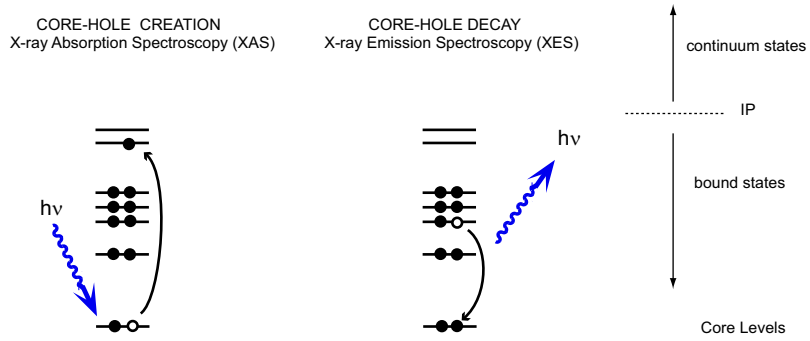

Figure 3.2: Illustration of XAS and XES as one–electron processes.

Another central feature of the x–ray absorption process is that the excitation of a core electron takes place on an extremely fast time scale (10^{-18}s); this means that XAS actually probes instantaneous configurations in dynamical systems like liquids. Because of its unique ability to provide a local and instantaneous picture of the electronic structure around single molecules in a dynamical system, XAS has provided new and somewhat surprising information about the structure of the first hydration shell of liquid water (see paper III).

According to the energy of the absorbed photon the core–electron can be excited into bound electronic states, below the ionization potential (IP) or in the continuum region above the IP (See figure 3.2). The states below the IP can be interpreted as valence or Rydberg states and usually give rise to rather sharp features in the spectrum. In the surface–sensitive XAS spectra of ice (shown in figure 3.3) the sharp pre–edge peak at 535 eV is for example assigned to a σ^* orbital localized along the internal O–H bond direction when the donating hydrogen–bond is broken (See paper X for the discussion of the XA spectra of ice). In the continuum region above the IP all features show up as broad peaks, some of which being assigned to multi–electron excitations, the so–called shake–up processes, or to the so called "shape resonance". The shape resonance occurs when the excited electron is trapped in the molecular potential barrier for a short period before being able to leave the system. The position of the shape resonance has been successfully correlated with the adsorbate–substrate bond length in the empirical "bond length with a ruler" model [81, 83], where bond lengths are determined simply by extrapolation knowing that the shape resonance shifts to lower energies as the bond gets longer. In paper IV the "bond length with a ruler" is used to relate the position of the broad band in the continuum region in the simulated ice spectra (see figure 3.3), assigned to water molecules with both HBs at the donor side intact, to the hydrogen bond (oxygen–oxygen) distance.

Another interesting aspect of XAS comes with the fact that different techniques for the detection of the absorption cross–section, characterized by different probing depths [84], are available and thus we can selectively obtain spectral contributions coming from the surface or deeper within the bulk of a material. Both emitted photons (in the radiative process), ejected (Auger) electrons (non-radiative process)

and even ions, generated in the core–hole decay, can be detected. The radiative yield has weak intensity for light elements like oxygen but has a large probing depth ($\sim$ 10 μm). The Auger electrons instead have much shorter mean escape depths, making the non–radiative yield inherently surface sensitive. Because the electron yield dominates the decay this detection technique is of common use in surface science. Furthermore, electrons characterized by different kinetic energies have slightly different probing depths. For water low energy electrons (Secondary electron yield, SEY) can probe as deep as 50 Å while faster electrons (Auger electron yield, AEY) can travel no longer than 20 Å in the bulk before energy loss events. A way to obtain truly bulk–sensitive (with penetration depths on the order of 0.15 mm) absorption spectra is to turn to x–ray Raman Scattering (XRS) [85, 86]. In an XRS experiment the hard x–ray incident photon is inelastically scattered and a small amount of energy is transferred to the sample. The high energy of the hard x–ray photons permits electronic excitation of core levels, so that XRS still yields all XAS information. At the opposite extreme, spectra primarily sensitive to the outermost surface layer (1–5 Å) [87] can be obtained by measuring the total ion yield (TIY), i.e. the ions ejected into the vacuum due to the dissociation resulting from core excitation. TIY is used in papers II and VIII to selectively study the local structures of the molecules at the liquid/vapor interfaces of water and methanol.

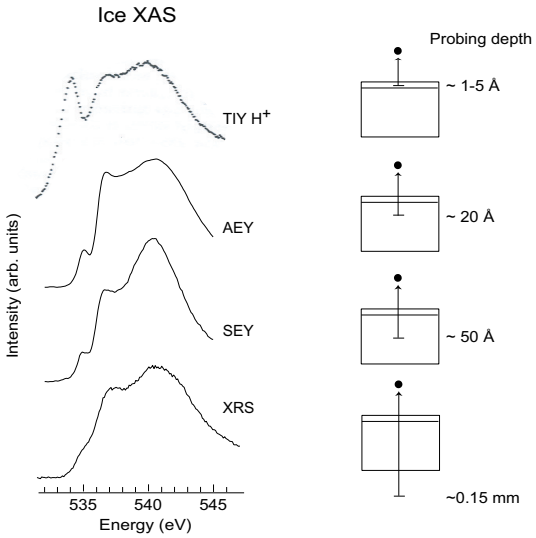

Figure 3.3: XAS of Ice measured with different detecting techniques together with the respective probing depth. The surface sensitive spectrum (TIY, taken from ref. [88]) is dominated by molecules with one free OH, which is reflected by the pronounced pre–edge peak. The intense continuum peak at $\sim$ 540 eV in the XRS and SEY spectra arises from the near–tetrahedral coordination of the water molecules in the bulk.

The capability of XAS to probe different regions of a sample, determined by the relative escape depths of the detected particles is summarized, for the case of Ice, in figure 3.3; molecules with a free O–H bond, like those in the top monolayer

of the surface of Ice, are characterized by the sharp pre–edge peak at $\sim$ 535 eV that vanishes in the spectra dominated by contributions from the bulk where each water molecule is fully coordinated in a near–tetrahedral configuration (for the full discussion of the dependence of XA spectral shape on the HB configuration and its implications for the local structure of liquid water see chapter 4.1.1 and also papers I through IV).

3.1.2 X–Ray Emission

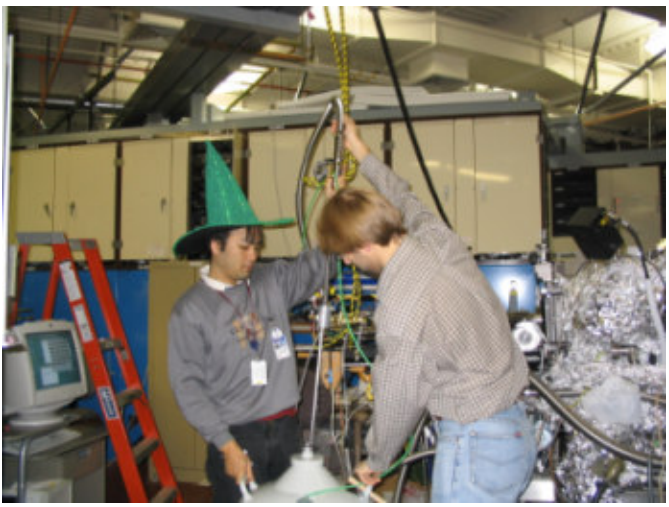

Figure 3.4: The wizardry of performing a synchrotron experiment. In the picture Hirohito Ogasawara (left) and Lars–Åke Näslund at beamline 8.0 of the Advanced Light Source, Berkeley, California.

XES probes the occupied valence states in an atom–specific projection by measuring the energy distribution of emitted photons from a core–hole decay, as schematically sketched in figure 3.2.

As discussed in the previous section, Auger electron decay will be the dominating process for light elements and fluorescence yields only about one photon emitted per 100 photons absorbed. For this reason such experiments require the use of non–conventional high intensity x–ray sources like those provided by 3rd generation synchrotrons.

The localization of the core–orbital makes XES local and atom–specific in a similar manner as XAS. Transitions from the valence states into the core–hole also follow the dipole selection rules, so that after an excitation from a core–orbital of s–symmetry only valence states of p–character are probed in the emission process [82].

In the non–resonant mode the core–electron is excited well above the IP in the continuum leaving a final state with one valence–hole, as depicted in figure 3.5. As a first approximation this means that the theoretical analysis can therefore be done using the ground state wavefunction making the simulation of XES spectra

within a self consistent field (SCF) framework formally very trivial, in contrast to the numerous challenges in obtaining the experimental spectra.

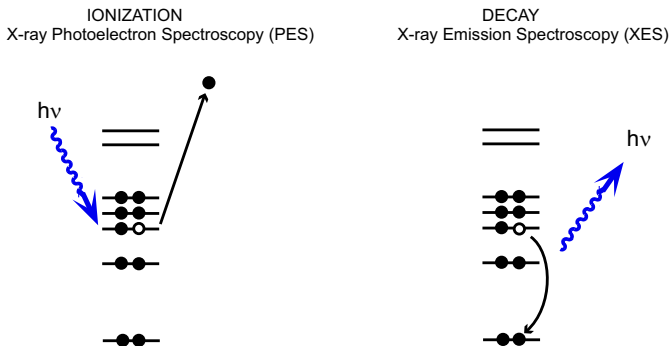

Figure 3.5: The same valence–hole final state in XES and PES, created by decay in the core–hole and direct photoionization.

In reality, because of the finite core–hole lifetime prior to the decay, the XES analysis can be complicated by the dynamical effects in the motion of the nuclei induced by the core–excitation. It was recently demonstrated that XES measurements of ice carry information about ultrafast dissociation events of the ionized water molecule that take place on a time scale comparable to the O (1s) hole lifetime ($\sim$ 4 fs) [89].

The same valence–hole final state of XES can be reached through photo–emission spectroscopy [90] (PES) by direct photoionization of the valence states, as displayed in figure 3.5. Like in XAS, the excitation process in PES is instantaneous so that the dynamical effects can be neglected whereas they are expected to influence the outcome of a XES measurement. By varying the photon excitation energy, PES provides an important tool to obtain a direct atomistic population analysis; at high excitation energy the 2s–contribution dominates the spectral shape, while at relatively low photon energies the signal will present almost exclusively 2p–contributions. In fact, it can be demonstrated that XES and low–energy PES spectra would become nearly identical if no dissociation would occur during the XES core–hole lifetime. Thus we can theoretically evaluate the low–energy PES through computed XES spectra in the frozen ground–state and dipole approximations, as done in paper XI in order to investigate the nature of the hydrogen–bond in ice.

3.2 Density Functional Theory

In recent years, thanks to the availability of robust mathematical formalisms and outstanding developments in computer technology, the field of computational chemistry has blossomed from being the playground of a few scientists interested in ideal model systems to become one of the principal tools applied to an endless variety of problems in chemistry, biology and materials sciences. Nowadays, computer–aided chemistry offers fundamental contributions to the understanding

of reaction mechanisms [91, 92] and enzyme function [93], assists in the design and synthesis of new materials [94] and plays an important role in the interpretation and analysis of the data from an endless variety of experimental techniques. Combining theoretical spectrum simulations with the core–level spectroscopies described in the previous section has made it possible to analyze in detail the surface chemical bond for a wide range of adsorbates and bonding types [82]. In this thesis this approach is extended to the study of the hydrogen bond in liquids.

3.2.1 Introduction to Quantum Chemistry

The time–independent non–relativistic Schrödinger equation

$$\hat{H}\Psi = E\Psi \tag{3.1}$$

represents the mathematical base of computational quantum chemistry[1].

The energy of the system, described by the wavefunction $\Psi(\mathbf{r}_1, \mathbf{r}_2, \cdots \mathbf{r}_N)$, is then given by the expectation value of the Hamiltonian $\hat{H}$:

$$E = \frac{\left\langle \Psi | \hat{H} | \Psi \right\rangle}{\langle \Psi | \Psi \rangle} \tag{3.2}$$

The full Hamiltonian of a physical system describes all the interactions of the nuclei and electrons as well as their kinetic terms. The corresponding Schrödinger equation becomes too complicated to be exactly solved but for very simple model problems and certain approximations are therefore required to make practical use of the quantum mechanical formalism.

The basic approximation is the so–called Born–Oppenheimer approximation [96], from the name of its proposers. It separates electron and nuclear motion based on the idea that nuclear mass is so much larger than electron mass that nuclear and electronic kinetic energy cross terms can usually be neglected and the nuclei considered to be "fixed" particles from the electrons' perspective. Thus the electronic structure is obtained for constant nuclear positions, which leads to the separation into electronic and nuclear the Schrödinger equations.

Beyond the Born–Oppenheimer approximation further simplifications are necessary to solve the electronic Schrödinger equation for many–body systems. One of the most basic in quantum chemistry is the Hartree–Fock (HF) method [97, 98] which assumes that electrons in the atom can be described as moving in the average field generated by the other electrons, thus neglecting the instantaneous pairwise correlation between them. A single electron is therefore associated with a one–electron wavefunction $\phi(\mathbf{r})$ depending on the spatial coordinates and the spin of the particle. The solution of the Schrödinger equation is taken to be of the form of a single Slater determinant of the N (where N is the total number of electrons) one–electron wavefunctions:

[1] This section aims to provide only an introduction to the basic aspects of quantum chemical theory. There are several textbooks the serious reader can refer to for a comprehensive and detailed description of the mathematical foundations of quantum chemistry and the Hartree–Fock method, the best probably being "Modern Quantum Chemistry" by Szabo and Ostlund [95].

$$\Psi(\mathbf{r}_1, \mathbf{r}_2, \cdots \mathbf{r}_N) = \frac{1}{\sqrt{N!}} \begin{vmatrix} \phi_1(\mathbf{r}_1) & \phi_2(\mathbf{r}_1) & \cdots & \phi_N(\mathbf{r}_1) \\ \phi_1(\mathbf{r}_2) & \phi_2(\mathbf{r}_2) & \cdots & \phi_N(\mathbf{r}_2) \\ \phi_1(\mathbf{r}_3) & \phi_2(\mathbf{r}_3) & \cdots & \phi_N(\mathbf{r}_3) \\ . & . & . & . \\ . & . & . & . \\ . & . & . & . \\ \phi_1(\mathbf{r}_N) & \phi_2(\mathbf{r}_N) & \cdots & \phi_N(\mathbf{r}_N) \end{vmatrix} \tag{3.3}$$

In this form the antisymmetry of the wave–function and thus the Pauli principle (which states that two electrons cannot be described by the same spinorbital) are guaranteed in the construction of the many–electron wavefunction.

Because each electron feels only the average field generated by the other electrons the Hartree–Fock method neglects the fact that the movements of the electrons are correlated, although the Slater determinant formalism guarantees the description of the exchange interaction, which means that a large fraction of the correlation of electrons with parallel spin is correctly accounted for.

The difference between the Hartree–Fock energy and the exact non–relativistic energy is therefore defined as correlation energy. Several theoretical techniques, some based on the variational principle, some on perturbation theory, have been developed through the years to approach the electronic correlation problem [99]. Although methods like the configuration interaction (CI) and coupled cluster (CC) provide very accurate evaluation of the energies (within the so–called chemical accuracy, 1–2 kcal mol^{-1}) the high computational costs limit their use to only relatively small systems.

3.2.2 The Kohn–Sham DFT Formalism

Historically, Density Functional Theory (DFT)[2] has provided an alternative approach to the wavefunction–based ones described above. The main idea of DFT is to use the electronic density, rather than the many-body wave function to describe a system of interacting electrons. For N electrons in a solid, which obey the Pauli principle and repel each other via the Coulomb potential, this means that the basic variable, the density $\rho(\mathbf{r})$ of the system depends only on three (the spatial coordinates x, y, and z), rather than 3*N degrees of freedom, which simplifies equation 3.1 tremendously.

Initially developed by Thomas and Fermi in the late 1920s [103, 104], DFT began its huge impact in computational chemistry in 1965 when Hohenberg and Kohn laid out their two fundamental theorems [105].

In the first theorem Hohenberg and Kohn use the variational principle to demonstrate that the electronic density $\rho(\mathbf{r})$ uniquely determines the external potential and therefore the total energy of the system. This has fundamental implications because it practically proves that all molecular properties can be determined by the electronic density. The second theorem shows that the ground

[2] Again, this is a quick introduction to the density functional theory; a deeper description can be found in the classic book by Parr and Yang [100] or in the beautiful reviews by Handy [101] and Labanowski [102].

state density can be calculated, in principle exactly, using the variational method involving only the density.

Therefore we may represent the electronic energy as a functional of the density:

$$E[\rho] = T_e[\rho] + V_{ext}[\rho] + U_{ee}[\rho] = T_e[\rho] + \int \rho(\mathbf{r})\hat{V}_{ext}(\mathbf{r})d\mathbf{r} + U_{ee}[\rho] \tag{3.4}$$

with T_e, kinetic energy of electrons, V_{ext} the external potential of the nuclei felt by the electrons and U_{ee}, the energy of interaction among electrons which contains a pure Coulomb ("classical") interaction and the exchange and correlation contributions, $E_{xc}[\rho]$,

$$U_{ee}[\rho] = \int \rho(\mathbf{r})U_{cl}(\mathbf{r})d\mathbf{r} + E_{xc}[\rho] \tag{3.5}$$

The form of the external potential is known:

$$\hat{V}_{ext} = \sum_{\alpha} \frac{-Z_\alpha}{|\mathbf{R}_\alpha - \mathbf{r}|} \tag{3.6}$$

(Z and R represent the nuclear charge and coordinates, respectively) as well as the Coulomb part of the interaction between the electrons, $\hat{U}_{cl}$:

$$\hat{U}_{cl}(\mathbf{r}) = \int \frac{\rho(\mathbf{r}')}{|\mathbf{r}' - \mathbf{r}|}d\mathbf{r}' \tag{3.7}$$

Unfortunately, the expression relating the kinetic energy T_e to the density is not known with satisfactory accuracy. Kohn and Sham's idea was to replace the T_e term with the kinetic energy of the corresponding non–interacting system, $T_0[\rho]$, which can be calculated exactly from a determinantal wave function for N non–interacting electrons in N orbitals ϕ^{KS} [106]:

$$\rho(\mathbf{r}) = \sum_{i=1}^{N} |\phi_i^{KS}(\mathbf{r})|^2 \tag{3.8}$$

$$T_0[\rho] = -\frac{1}{2}\sum_{i=1}^{N} \left\langle \phi_i^{KS} | \nabla_i^2 | \phi_i^{KS} \right\rangle \tag{3.9}$$

The energy functional 3.4 can now be rewritten in the Kohn–Sham formalism as:

$$E[\rho] = T_0[\rho] + \int \left[\hat{V}_{ext}(\mathbf{r}) + \hat{U}_{cl}(\mathbf{r})\right] \rho(\mathbf{r})d\mathbf{r} + E_{xc}[\rho] \tag{3.10}$$

The $E_{xc}[\rho]$ term, called exchange–correlation functional, includes all the energy contributions which were not accounted for by the previous terms, i.e. electron exchange, electron correlation (since interacting electrons do need to correlate their movements) the portion of the kinetic energy needed to correct $T_0[\rho]$ to obtain the true kinetic energy of a real system $T_e[\rho]$, and the correction for self-interaction introduced by the classical Coulomb potential.

At this point, it is worth noting that DFT yields the existence proof for the possibility of accurate results, provided that the exact expression of the exchange–correlation functional can be known. Unfortunately this is still unknown and there is no straightforward way in which the $E_{xc}[\rho]$ functional can be systematically improved. The simplest approximation to the $E_{xc}[\rho]$ functional is the local density approach (LDA) using the local form of the exchange–correlation, known exactly for a homogeneous electron gas [106, 107],

$$E_{xc}[\rho] = \int \rho(\mathbf{r})\epsilon_{xc}[\rho(\mathbf{r})]d\mathbf{r} \tag{3.11}$$

In other words in LDA the exchange–correlation at point $\mathbf{r}$ depends only on the density at $\mathbf{r}$. LDA exibits good results when applied to bulk materials but it is not adequate for useful predictions in systems in which the density varies rapidly, e.g. in molecules or at an interface with vacuum. Improvements over LDA are obtained with the generalized gradient approximation (GGA) functionals

$$E_{xc}[\rho] = \int \rho(\mathbf{r})\epsilon_{xc}[\rho(\mathbf{r}), \nabla\rho(\mathbf{r})]d\mathbf{r} \tag{3.12}$$

which introduce the necessary inhomogeneity in the electron density by adding in the functional new terms which depend on the gradient of the density at $\mathbf{r}$. Recently higher order gradient corrections (meta–GGA [108]) have also been proposed. GGA functionals, like Becke [109], PW86 [110] and BLYP [111], yield results with accuracy comparable to high–level *ab initio* methods at a much lower computational cost [101]. In fact, while linear–scaling can be achieved in some cases with DFT, the evaluation of multi–centers matrix–elements makes post–HF approaches to scale at best as N^4 with the problem size. A very popular class of functionals is the so–called "hybrid functionals", which is based on some semi–empirical mixing of the non–local HF exchange energy with the local exchange–correlation functionals previously discussed. The use of such functionals, like B3LYP [112] brings some further improvement in the accuracy of the computed energies in DFT but requires the explicit evaluation of the two–electron exchange integrals, at an increasing computational cost.

It should also be noted that non–local exchange–correlation effects, like those between non–overlapping electronic densities in van der Waals interactions, are not included in functionals of the present type which depend only locally on the density, although some attempts in this direction have recently been made [113–115].

3.3 Spectra Calculations

3.3.1 X–Ray Absorption

The x–ray absorption spectral intensity (or oscillator strength) of an atom or molecule can be calculated from Fermi's "Golden Rule" for the transition probability per unit time P_{if} from a state $|\Psi_i\rangle$ to a state $|\Psi_f\rangle$ driven by a harmonic time–dependent perturbation $V(t) = \overline{V}\ e^{-i\omega t}$ [81],

$$P_{\mathrm{if}} = \frac{2\pi}{\hbar} \mid \langle \Psi_{\mathrm{i}} | \overline{V} | \Psi_{\mathrm{f}} \rangle \mid^2 \rho_{\mathrm{f}}(E) \tag{3.13}$$

where $\rho_{\mathrm{f}}(E)$ is the energy density in the final state.

In the dipole approximation, which is valid if the wavelength of the incoming photon is much larger than the dimension of the system interacting with the light[3], the equation 3.13 can be simplified to obtain an expression of the spectral intensity much easier to handle:

$$I_{\mathrm{if}} = \frac{2}{m\hbar\omega} \mid \langle \Psi_{\mathrm{i}} | \overline{e} \cdot \overline{p} | \Psi_{\mathrm{f}} \rangle \mid^2 \tag{3.14}$$

where $\overline{p}$ is the sum of the linear momenta of the electrons and $\overline{e}$ is the polarization vector. The dipole transition element in this form is usually referred to as the "velocity" form.

By employing operator equivalents for the total linear momentum operator $\overline{\hat{p}} = \frac{im}{\hbar} [\hat{H}, \overline{r}]$ it is alternatively possible to write the matrix element using the "dipole operator" $\mu = \mathrm{e}\mathbf{r}$, in the so–called "length" form. The "length" gauge is valid if Ψ_{i} and Ψ_{f} are exact eigenstates of the total electronic Hamiltonian; for approximate wave–functions the accuracy of the matrix elements is related to the quality of the wave–functions, which is found to be sufficient for DFT but not necessarily so for all systems in HF. In the case of water it is demonstrated, as shown in paper V, that spectra calculations performed with DFT using the transition potential approximation described below, in the "length" and "velocity" framework give equivalent results.

The spectral intensity in "length" form is then determined by the dipole transition moment between the initial and the final state (separated by the energy difference $\hbar\omega_{\mathrm{if}}$):

$$I_{\mathrm{if}} = \frac{2}{3} \omega_{\mathrm{if}} \mid \langle \Psi_{\mathrm{i}} | \overline{\mu} | \Psi_{\mathrm{f}} \rangle \mid^2 \tag{3.15}$$

In order to simulate the XA spectrum, a set of energy levels and their corresponding oscillator strengths has to be determined; in the general case this leads to a state–by–state determination of the excited state wave functions and the evaluation of the cross sections between non–orthogonal wave functions. Because of the localization of the core–hole on one atomic site the absorption process can be reduced to a single–particle model, as depicted in fig.3.2. In this picture the XA spectrum reflects the local unoccupied density of states (DoS) and can be obtained entirely within DFT, including valence, Rydberg and continuum excitations, using the same wavefunction for the initial and final states. In other words, the core–hole state is used to define the potential for the unoccupied levels and the occupied orbitals are not relaxed in the presence of the excited electron. This results in a simplified evaluation of the transition element in terms of transitions involving the core orbital, typically a 1s orbital, $\phi_{1\mathrm{s}}$, and an unoccupied orbital (for the XA spectra) ϕ_{f}:

[3]For excitations of the oxygen 1s–shell at $\hbar\omega = 550$ eV the wavelength $\lambda/2\pi = 3.6$ Å and the K–shell diameter can be estimated from the Bohr radius $\mathrm{a_o} = 0.53$ Å and the atomic number Z as $\mid \mathbf{r} \mid \approx 2a_{\mathrm{o}}/Z = 0.13$ Å, so that the dipole approximation is well satisfied.

$$I_{\rm if} = \frac{2}{3}\,\omega_{\rm if} \mid \langle \phi_{\rm 1s} | \overline{\mu} | \phi_{\rm f} \rangle \mid^{2} \tag{3.16}$$

This approach is very similar to the static–exchange (STEX) used to generate XA spectra from Hartree–Fock wavefunctions [116]. In the STEX, the orbitals describing the one–electron excitations are obtained as eigenvectors of a one–particle Hamiltonian constructed from the orbitals of the fully relaxed molecular ion core with the appropriate spin state (doublet for a closed–shell ground state). In the HF STEX method the non–orthogonal transition moments between the ground and final states are computed but the description of the dynamical correlation, which is instead defined in the functional formalism of DFT, is missing.

According to the initial and final state rules [117–119], the spectral shape is determined by the eigenstates of the final state Hamiltonian which include the core–hole in XAS, as represented graphically in fig.3.2. The total transition intensities are instead given by the number of unoccupied levels in the initial state, before the x–ray transition takes place, which for XAS corresponds to the ground state. In order to analyze the experiments by means of theoretical modeling it is important to understand the influence of the core–hole, or in other words to find the right balance in the chosen theoretical approach between the initial and final state effects.

Historically a way to generate theoretical XA spectra has been the Z+1 or the equivalent full core–hole (FCH) approximation which implies that the core–excited atom is replaced by an atom of the element following it in the periodic table. In XA spectrum calculations this can be done by removing a core electron [120, 121] (in all–electron calculations) or by specially designed pseudopotentials with occupation $1s^1$ [122, 123] (in e.g plane–waves–based spectrum calculations). The FCH wavefunction corresponds to the fully relaxed core–hole state of the molecule but neglects completely the effects of the initial state.

An alternative approach is the transition potential (TP, or half core–hole, HCH) approximation in which half a core–electron is excited in the calculation [120, 124, 125]. This technique is easily implemented in the DFT Kohn–Sham framework. Unlike Hartree–Fock orbitals, Kohn–Sham orbital[4] energies lack a direct physical interpretation as ionization potentials. The connection to the orbital binding energy is instead through a derivative of the total energy with respect to changes in orbital occupation numbers, $n_{\rm i}$:

$$\epsilon_i = \frac{\partial E}{\partial n_i} \tag{3.17}$$

There are pragmatic reasons for preferring the transition potential approximation to XA spectrum generation. The argument is that in this way initial and final state contributions are treated in a balanced manner; moreover it has been proven by Taylor expansion that the final state relaxation effects are taken care of up to the second order for occupation number $n_{\rm i} = 0.5$. The transition potential

[4] Although they are constructed to reproduce the density of a non–interacting electronic system (see equation 3.8), the KS orbitals resemble in shape the HF ones and retain, against all odds, the same interpretability.

approach has been successfully applied to free molecules [126], the adsorption of various molecules, including glycine [127] and octane [128] on metallic surfaces and, in this thesis, to hydrogen–bonded liquids. Applications to gas phase pyridine [126] and chemisorbed glycine [127] show the accuracy obtainable with this approach. On the other hand, the full core–hole approximation provides a better description of systems in which the final state effects are dominant, as in the case of the C K–edge spectrum of fullerenes [129], where core excitons are important in the formation of the XA–states, so that the use of the HCH or the FCH method should be considered on a case–by–case base.

A way to include both initial and final state effects is provided by the ΔKohn–Sham (ΔKS) method [120,126,130] where the orbital binding energies are obtained as energy differences between the neutral ground state and the corresponding resonant core–excited states. For small molecules, like gas–phase pyridine [126], this procedure yields excellent results.

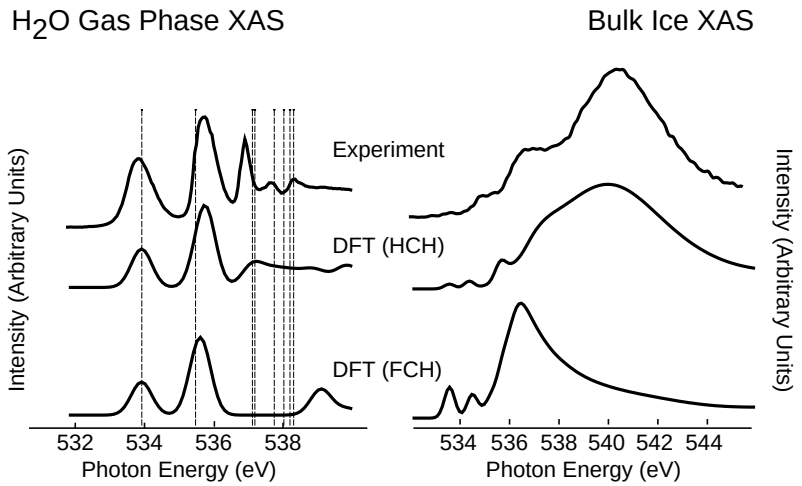

Figure 3.6: XAS spectra of the H_2O isolated molecule (left) and bulk ice (right) calculated using the HCH and the FCH approximations of the core potential. The vertical dashed lines represent the energy positions of the first eight transitions computed with the ΔKS method. The experimental spectra are taken from paper III.

Paper V investigates the effects of different core–potentials in the calculation of XA spectra of water. In terms of absolute energy scale the FCH calculations produce errors on the order of 10–15 eV with respect to experiment, compared with 1–3 eV as typical for the HCH approximation.

Figure 3.6 summarizes the results of this investigation by comparing the computed spectra of gas phase water and ice calculated with the HCH and FCH potentials with experiment. To fairly compare the half and full core–hole approaches the spectral energy scale was corrected through the ΔKS method where the XA spectra are uniformly shifted by matching the lowest excited state to the energy difference between the total Kohn–Sham energies of the first resonant core–excited state and the ground state cluster.

The transition potential represents a more balanced compromise between the

effects of the initial and final states in the case of water and compares favorably with the experimental spectra of bulk ice, ice surface and the gas phase, which, as discussed in section 2.3, represent experimental models for water in different hydrogen bonding situations (two, one and no donating HB, respectively), and with the excitation energies computed with the ΔKS method in the case of the isolated molecule. Instead the FCH approach provides a better description of systems where well localized core–excitons are fundamental, but it is shown to overestimate these effects when the excited electron rapidly delocalizes in band–type structures. In the case of water, and particularly in ice, this provokes the localization and the lowering of the band states resulting in an XA spectrum lacking intensity at 540 eV (broad band signature of an intact donating HB) with excess intensity in the pre–edge region. In the gas phase molecule the Z+1 approximation exaggerates the localization of the 2p orbitals, enhancing the screening felt by the 3p and the series of Rydberg states that will be shifted to higher energy, resulting in poor agreement with the experimental spectrum.

As seen in this section calculation of x–ray absorption spectra in the FCH and HCH approximations requires the description of excited electronic states, and it is often argued, since the proof of the uniqueness of the external potential arising from a density ρ is obtained applying the variational principle, that DFT is only applicable to the ground state. Instead it is possible to show that the validity of the DFT method extends far beyond the ground state. The proof of the uniqueness of the energy functional relies on an application of the variational principle and as such can be derived also for any well–defined state that is bounded from below, e.g. core–excitations and excitations from the highest occupied molecular orbital (HOMO). In cases where the orbital from which the electron is excited is well separated from the rest of the occupied orbitals we can always apply the variational principle to obtain the lowest state in a restricted variational space. Considering x–ray absorption we can thus variationally determine the lowest core–excited state using the constraint that the core–level in question should contain only one (in the FCH approximation) or one and a half (in the TP formalism) electron [126]. What has been delineated above is naturally not applicable for cases where the requirement of well–separated initial orbitals for the excitation is not met; for such cases only the more general time–dependent DFT (TDDFT) approach can be expected to give reliable results.

3.3.2 X–Ray Emission

For XES the transition intensities are computed as the square of the matrix element of the dipole transitions from an occupied valence state into the core–hole. Similar to the method described for XAS in section 3.3.1 we can use the same potential, obtained from the ground state wavefunction, to describe both the initial and different final states. The KS orbital energies are used as binding energies for the occupied valence state.

The use of the ground state orbitals in the calculations of the XES transition moments gives good agreement with experiment [82, 131] and the use of the transition potential method or the FCH approach does not necessarily improve the description [132]. This is somewhat surprising since the XES process is inter-

preted in a simple one–electron picture as the radiative decay of a valence electron into a core–vacancy created by a previous core–excitation, as depicted in fig. 3.2, so that the core–hole relaxation effects are expected to largely affect the spectrum. In practice the ground–state approximation for XES gives good results due to the cancellation of errors by neglecting both core and valence relaxation effects [131, 132].

In this static approach both vibrational information and excited state nuclear dynamics (e.g. core–induced dissociation of the molecule during the core–hole life time) are neglected. The core–induced dynamics can by captured by *ab initio* molecular dynamics [89] and it is shown to have a large effect on the XE spectra of ice and gas phase water. The correct inclusion of dynamical core–hole effects improves the agreement with experiment, particularly in terms of intensity ratios of the peaks.

In papers X and XI a simple r^2 operator is used to obtain the s–projected states; although it does not correspond to any physical operator, it does provide a convenient description of the s–density of states around the excited center. In paper XI this s–contribution is added to the p–projected density of states in order to generate theoretical PES spectra. Since the r^2 operator does not provide an absolute intensity its contribution to the high energy PES is chosen arbitrarily, while the low–energy spectrum is scaled with relative weight according to the relative 2p and 2s atomic cross–sections for oxygen obtained from reference [133].

3.3.3 Computational Details

The transition potential method is used to generate XA spectra throughout the thesis. In all papers the spectra calculations are performed using the StoBe deMon DFT program [134], using the theoretical scheme described above in equations 3.15 and 3.16.

The core–excited atom, placed in the center of the cluster, is described using the Iglo–III all-electron basis set of Kutzelnigg [135], allowing for the relaxation of the core–hole, while all other centers of the same type are described by effective core potentials (ECP) [136]. This procedure allows us to safely locate the core–hole on the atom of interest; careful checks against all–electron calculations have been performed [137] showing no changes in spectral shape and only minimal (on the order of 0.1 eV) energy shifts due to the use of ECPs.

Delocalized unoccupied states, like those composing the Rydberg series and the continuum band, are poorly described by a small orbital basis set. In order to improve the treatment of these states we employ a double basis set technique where the normal molecular basis set is augmented by a large diffuse basis ($\sim$ 150 functions) after the energy minimization for the evaluation of the transition moments and the excitation energies [120, 138].

The XA spectra for ice and water are generated based on the discrete oscillator strengths computed in equation 3.16. These are convoluted to form the absorption spectrum using Gaussian functions of constant full–width–at–half–maximum (fwhm) of 0.5 eV below 537.5 eV then linearly increasing up to 8 eV at 550 eV; at higher energies the fwhm is constant. This approach was used throughout this

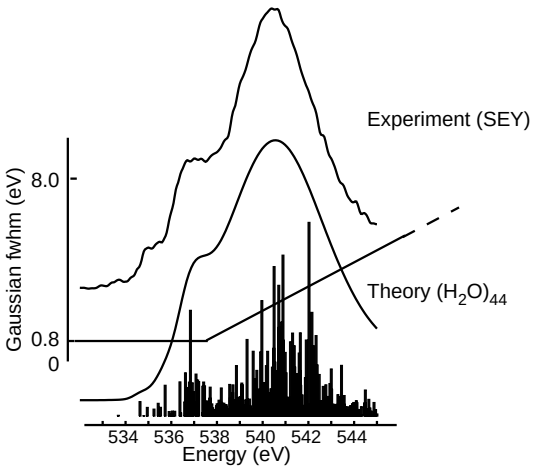

Figure 3.7: The convolution scheme for XAS.

thesis to mimic the experimental broadening of the transitions, which has instrumental, vibrational as well as lifetime origin, and to ease the visual comparison with experiment. Although the correct experimental broadening cannot easily be determined, it is known that excitations in the bound states below the IP are typically dominated by vibrational and lifetime broadening in the order of 1 eV or less. Above the IP the broadening is dominated by the very short lifetime of the excited state and a linear increase of the broadening function up to the continuum band gives a good representation of the phenomenon. With this in mind we have developed the described convolution scheme by fitting the experimental hexagonal ice (Ih) XA spectrum with a spectrum calculation using a large (44 water molecule cluster) model, as depicted in figure 3.7.

In the x–ray emission process it is the vibrational contributions that dominate the experimental broadening and as such the theoretical spectra are convoluted with Gaussians of constant 0.5 eV width.

In paper VI we describe a new method to compute XA spectra in a periodic plane–waves DFT framework. The spectra calculations are carried out with the CPMD code [139] using the transition potential technique with the effect of the core–hole included through a specifically designed pseudo–potential with fractional occupation in the ϕ_{1s} orbital on the excited atom. Because of the lack of the ϕ_{1s} orbital in the pseudo–potential framework the XA spectra can be calculated directly only on a relative energy scale. To obtain the necessary absolute energy scale we instead use the 2s–level, knowing that the fluctuations in the computed energy difference between the ϕ_{2s} and the ϕ_{1s} levels are rather small. In fact the average energy difference E(ϕ_{2s} - ϕ_{1s}) of 508.48 eV calculated in paper VI for several hundred liquid water clusters using the all–electron DFT approach is found to have a standard deviation of only 0.30 eV, validating our approach. Alternatively a somewhat arbitrary shift on the energy axis needs to be applied to the theoretical spectra obtained in the plane–waves pseudopotential framework for comparison with experiment [122, 123].

For all local basis set calculations the exchange contribution developed by

Becke [109] is used together with the PD86 [110] correlation functional[5]. This level of theory is well tested for x–ray spectroscopy calculations and gives reliable results for many adsorbate systems [128,131,140–145]. In the periodic calculations the Becke exchange is instead associated with the LYP [111] correlation functional; however it has been proven that core–excitation energies are largely dependent on the choice of the exchange and rather insensitive to the correlation functionals [146]. Moreover the relative transition energies are rather stable with respect to the choice of functionals and the XA spectra computed with the cluster and the periodic approaches are in good agreement with each other (See paper VI).

[5]It has to be pointed out here that the StoBe deMon DFT–code [134] used in this thesis does not include the possibility to compute the HF exchange which is central to the description of hybrid functionals like B3LYP.

Chapter 4

Summary of the Main Results

The core level spectroscopies owe their success in fields such as surface and material science to the capability to supply direct and instantaneous information on the local occupied (e.g. XES) and unoccupied (probed by XAS) valence electronic structure. When a molecule interacts with its neighbors it is the valence space that undergoes changes, the extent and nature of which are related to the type of interaction and to the relative positions of the molecules in space. Hence, by probing these changes, core level spectroscopies also yield indirect but accurate information about the geometry of the system. This chapter is devoted to a brief summary of the understanding of the geometrical and electronic structure of H–bonded liquids, gained here from the strict combination of core level spectroscopies and DFT calculations.

4.1 Geometrical Structure

4.1.1 Liquid Water

As anticipated in section 2.2 changes in the valence electronic structure of water are also expected upon hydrogen–bond formation. In this light it is not surprising to find, as described in paper I, that the XA spectrum of gas phase water differs strongly from that of ice and liquid water.

The gas phase spectrum, shown in figure 4.1, exhibits well separated peaks corresponding to the O(1s) excitations into the antibonding O–H $4a_1$ and $2b_1$ orbitals[1] at low–energies (534–536 eV) and transitions into the Rydberg series at high energies (537–539 eV). As water condenses the spectrum broadens into a conduction band (537–539 eV) whose shape will be shown to be strongly dependent on the type and the strength of the HB configuration adopted locally by the water molecules.

[1] we point to figure 2.1 for the graphical depiction of the molecular orbitals of the isolated water molecule.

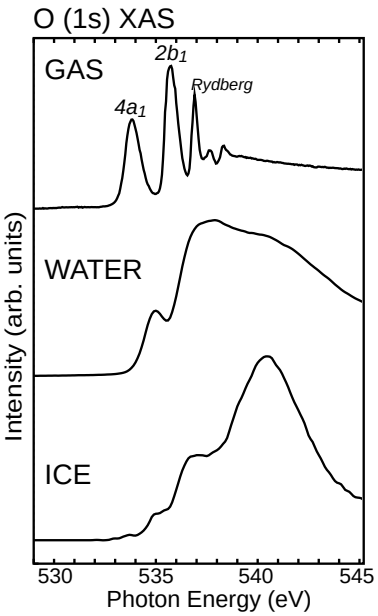

Figure 4.1: Experimental XAS spectra of bulk ice (SEY), liquid water (fluorescence yield and corrected for saturation effects) from paper III and gas phase from paper I.

The measured spectra of liquid water and ice, displayed in figure 4.1, also manifest considerable differences from each other; in the solid state the XA signal is characterized by a pronounced structure in the continuum ($\sim$ 540.5 eV) but lacks the sharp pre–edge (535 eV) and the enhanced intensity of the main edge feature (537 eV) compared to that of the liquid. Prior to our experiments the different distribution of intensities in the conduction band of water and ice was noted through XRS data [147], although without the resolution needed to resolve the pre–edge region in the liquid phase spectrum.

It is at this point worthwhile to note that these differences in the spectra are unexpectedly large if one should consider the local arrangement of water molecules in the liquid as simply a mere distortion from the tetrahedral configuration of ice.

In paper I we rely on DFT calculations for the interpretation of the spectral features in the liquid signal in terms of different possible structural contributions, with particular emphasis given in this phase to the origin of the sharp pre–edge peak. We compute the spectra of several model structures, representing typical HB configurations in liquid water, generated from a classical MD simulation [148]. The excited water molecule is placed at the center of a cluster consisting of at least its complete first and second hydration shells, with an average size of $\sim$ 30 water molecules.

The results of the spectra calculations are summarized in figure 4.2. It is found that the sharp pre–edge is due to molecules which have an uncoordinated O–H bond, while molecules with both their donating HBs intact produce spectra that do not significantly deviate from that of ice. Instead, the computed spectra are

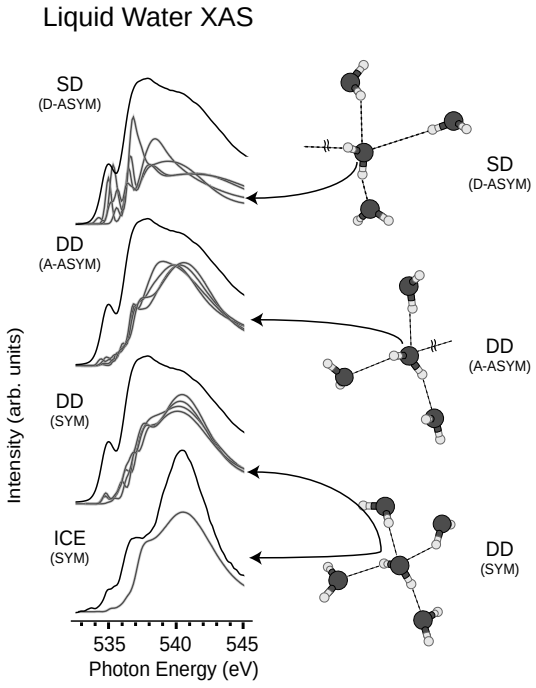

Figure 4.2: Calculated XAS spectra of ice (44 H_2O cluster) and of three typical HB configurations: fully coordinated (SYM,DD), broken HB at the H-side (SD) and lacking an accepting HB (ASYM or DD in the nomenclature in paper III and used throughout the thesis). For each of the above categories, four spectra corresponding to typical variations in distances and angles are shown. The experimental spectra of water and ice are shown above each set of simulated spectra.

only negligibly affected by the coordination of the water molecules at the lone–pair side, so that configurations characterized only by differences in accepting HB coordination are indistinguishable in XAS. Note that in figure 4.2 we choose to categorize the different molecule classes employing the nomenclature introduced in paper III instead of the one given originally in paper I in order to provide a uniform discussion throughout the thesis. Since they present common spectral fingerprints, regardless of the number of HBs at the accepting side, molecules with both O–H coordinated are defined as double–donor (DD), while molecules lacking a donating HB, characterized by the sharp pre–edge peak in the spectra, are classified as single–donor (SD) species.

Paper II describes the measurements of the XAS of a thin liquid jet of water, summarized in figure 4.3. This technique, coupled with the enhanced surface sensitivity of the TIY detection method (see section 3.1.1 and specifically figure 3.3), allows the characterization of molecules in equilibrium with the gas at the liquid–vapor interface.

The resulting spectrum, after the corrections needed to account for the water vapor contribution to the signal, appears very different from both those of liq-

uid water and ice. Instead of the broad band that characterizes the spectra of the condensed phases, the TIY exhibits fully resolved $4a_1$, $2b_1$ and the first of the Rydberg peaks that are $\sim 10\%$ broader and unshifted in energy relative to their gas–phase analogues. The rest of the Rydberg series, on the other hand, is broadened to a single band which merges into the continuum.

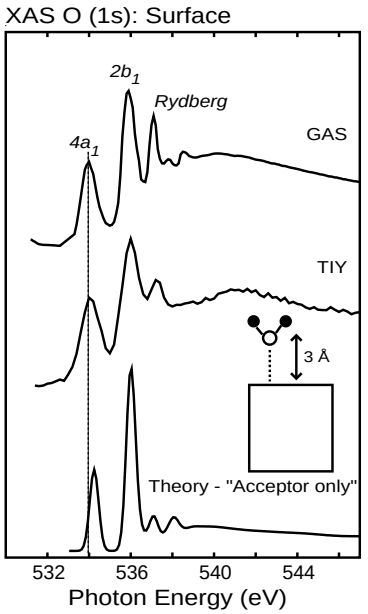

Figure 4.3: XAS spectra of water: gas phase, TIY spectrum obtained from a 20 μm diameter liquid jet and calculated for a "single acceptor" molecule, schematically shown on the right end side of the figure. The cluster for the calculations contained 30 water molecules.

Models of the liquid surface for the spectra calculations were obtained by constructing specific clusters wherein the interfacial water molecule in different coordination environments is situated at 3 Å O–O distance to the liquid surface, as deduced from EXAFS in the surface region [53].

The calculations clearly identify a previously unrecognized type of "acceptor–only" species with two free O–H groups (non–donor, ND, molecules in the notation of paper III) at the surface of water, in addition to the single donor configuration previously observed by SFG studies [52] and responsible for the broad feature at 541–543 eV. Recently these findings have been corroborated by an *ab initio* MD simulation reported by Kuo and Mundy [54], who find that 19% of the surface molecules are "acceptor–only".

Another important aspect worth noting is that, through the extensive similarities between the experimental spectra of the isolated H_2O and the "acceptor–only" species, we obtain further evidence of the sensitivity of XAS towards the HB coordination at the hydrogen side rather than at the oxygen side. Similarly the observation of the common characteristics of the absorption spectra of liquid wa-

ter and the surface of ice in figure 4.4 is suggestive of important clues to the local structural environment of water at ambient conditions.

In fact, as discussed in section 2.3, although the exact HB environment at the surface of ice still raises questions, there is a consensus that a large fraction of the molecules in the first bilayer of the ice Ih surface have one free O–H, whereas the rest point towards the bulk. As can be observed in fig. 4.4, the surface of ice and liquid water produce very similar XAS spectra, characterized by a sharp pre–edge peak, a dominant main—edge and less intensity in the post–edge region compared with bulk ice. Moreover, upon adsorption of an HB acceptor species like NH_3, we can achieve a coordination of the surface free O–H groups which results in the vanishing of the pre–edge peak and the shift of intensity to the post–edge region. These observations provide direct experimental validation of the correctness of the assignment, done in paper I on the basis of theoretical calculations, of the intensities in the pre- and main–edge regions to water molecules with one uncoordinated O–H (i.e. SD species).

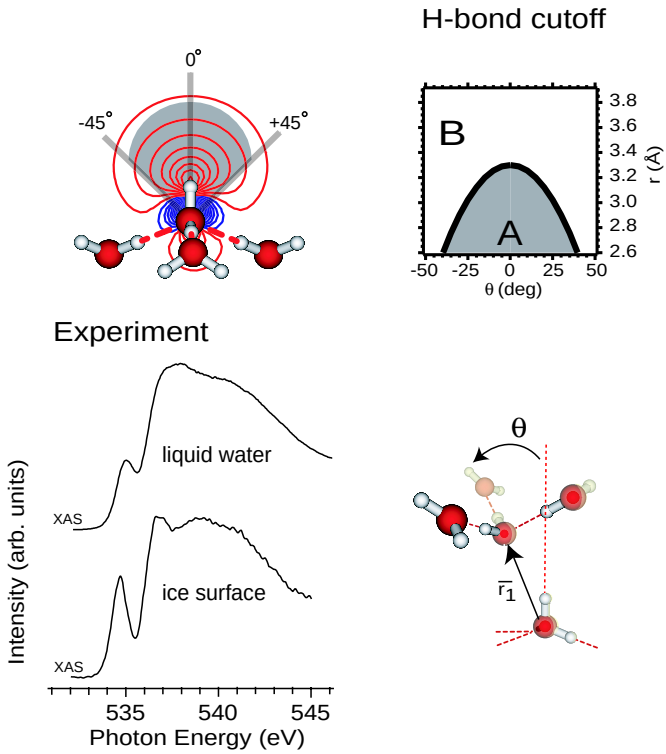

Figure 4.4: Experimental XAS of liquid water at ambient conditions and Ice Ih surface (AEY) (left, bottom). The orbital plot corresponding to the excitation in the pre–edge of a SD species (left, top). The geometrical representation of the HB cutoff cone described in the text (right).

Remarkably, the striking similarity of the XA spectrum of liquid water to that of the ice surface as opposed to bulk ice suggests that molecules in the bulk liquid

Type	FIT	MCYL [149]	SPC [150]	CPMD [139]
DD	15^{+25}_{-15}	50	70	79
SD	80±20	41	27	20
ND	5±5	9	3	1

Table 4.1: Relative amount of local configurations (DD, SD, ND) in liquid water at 25 °C according to different MD simulations and using the HB cutoff definition described in figure 4.4. The values in the right column are experimentally derived from XA spectra fitting. The errors are given by the uncertainties related to experimental observations and the limited size of the clusters used in the fitting procedure.

exhibit a local coordination with one strong and one broken or weakly bonded O–H group, comparable to that of the top bilayer of ice.

In paper III we use small model clusters of eleven molecules to systematically study the effects of hydrogen–bond elongations and distortions on the XA spectrum of water. Based on calculations on a large number of local configurations we define the HB cutoff in figure 4.4. The boundaries between the zones are based on the occurrence of the strong pre- and main–edge features (i.e. similar to the experimental ice surface spectrum) when the nearest neighbor is outside the gray zone beyond the black line. The "hydrogen–bond cone" defined in this way is used to classify the three groups of configurations in the liquid which give distinct XAS signals: DD species, with two–intact (i.e. both inside the gray zone) donating HBs, characterized by XA spectra with no pre–edge peak and strong post–edge intensity, SD molecules retaining the coordination of only one O–H bond and giving rise to strong pre- and main–edge peaks and NDs with both donor-HB broken presenting two distinct peaks similar to the spectrum of the gas phase water and the "acceptor only" interfacial species described in paper II. From an energetics point of view, calculations on the same eleven water molecules clusters at the MP2 level show that the hydrogen–bond strength at the boundaries of the gray cone is reduced to $\sim 40\%$.

In an orbital picture, as emerged from paper X, the pre–edge intensity corresponds to excitations into the unoccupied antibonding orbital localized along the internal O–H direction. This localization is caused by breaking the donating HB which leads to s–p rehybridization of the orbital and a corresponding enhancement of the p–character which translates to an increase of the intensity of the peak via the dipole selection rule. It is interesting to observe in fig. 4.4 how this antibonding molecular orbital closely matches the cone and thereby provides the physical basis for our HB cutoff; i.e. the orbital rehybridization provoked by a molecule as it approaches the shaded area and the corresponding change in the associated spectral feature.

Whereas the similarity between the experimental spectra of liquid water and surface of ice points undoubtedly to a structure of water in which most of the

molecules are in the SD configuration[2], it is necessary to try to fit the experimental data with a sum of computed spectra in order to estimate the fraction of DD/SD/ND species in liquid water. The results are summarized in table 4.1. It is important to note at this stage that, although the eleven water molecule clusters are able to reproduce all general shapes and trends of the experimental spectra, full convergence of the computed spectra with cluster size is not reached even for the largest models (~ 50 H_2O), as discussed in detail in paper VI.

This uncertainty related to the small dimensions of the cluster is reflected by the rather large errors allowed for the relative amounts of the different configurations from the experimental observations in table 4.1.

However, in order to be validated our findings must be able to adequately describe the RDFs[3], obtained from x–ray and neutron diffraction, data, which form a reliable yet only isotropically averaged set of structural information.

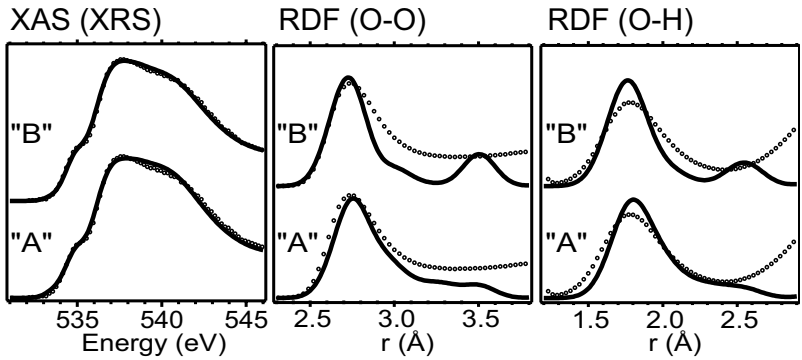

Figure 4.5: Calculated XAS and RDFs (solid lines) for the models "A" and "B" described in the text. Spectra and RDFs were generated for the central water molecules in clusters consisting of eleven water molecules, for a total of fourteen clusters. The computed XAS spectra were broadened with a 1 eV Gaussian for better comparison with the experimental XRS data. The experimental RDFs (open circles) are derived from neutron diffraction [44].

The models "A" and "B" in figure 4.5 use the same balance of clusters, representing DD/SD and ND species (10:85:5) consistent with the measured XAS data (see table 4.1). Model A has more angularly distorted HB and less elongated ones, while B has HB predominantly broken by elongation rather than bending. Both models reproduce the experimental XRS spectrum[4] but only A demonstrates good agreement with the RDFs within the first solvation shell. Model B instead

[2]Moreover, symmetry arguments imply that, with a dominant fraction of molecules with an unsaturated donating O–H bond, the majority of the waters must in addition have also a broken accepting HB, undetectable by means of XAS.

[3]Obviously the eleven molecule clusters, used in this analysis, are insufficient for a full description of the RDFs beyond the first solvation shell (~ 3.5Å for the O–O RDF) and hence we should not expect agreement at larger distances.

[4]Note that XRS and XAS essentially give the same information, as indicated by the similarity of the room–temperature water spectra in paper III. Their slight diffences are due to the poorer energy resolution of XRS.

overemphasizes the contribution at ~ 3.5 Å and lacks structural contributions in the region 2.9–3.3 Å of the O–O RDF.

Comparing XAS and diffraction data we therefore conclude that most molecules in liquid water are in asymmetrical HB configurations, with two strong and two broken or weak HBs (the hydrogen bond energetics is down to 40% at the cutoff boundaries), predominantly because of bending, rather than in distorted tetrahedral structures reminiscent of bulk ice. Such a local structure is also able to explain femtosecond–IR studies indicating the presence of two different O–H groups in water: one "strongly" and one "weakly" H–bonded [15]. Energetically we furthermore expect the intact hydrogen–bonds in the proposed SD configurations to be stronger than the average bond in the four–fold coordination due to anticooperativity effects [16, 151].

An experimentally determined average distribution of HB lengths and angles in liquid water over a wide temperature range has recently become available, through measurements of the anisotropy of the proton magnetic shielding tensor, determined through the field-dependence in the proton nuclear spin relaxation [49]. At room temperature a certain degree of distortion from linearity of the HB is found, although insufficient to be compatible with our formulated hypothesis of nearly 80% SD species in water. These results, which have also proven to be consistent with diffraction data, seem instead to agree with a slightly smaller fraction of SD configurations, possibly towards the lower end of the error bars given in table 4.1 (i.e. $\sim 60\%$ SD).

Finally, it is crucial to point out that a model of liquid water implying that the dominant fraction of the molecules are in configurations with asymmetric H–bonding (i.e. one strong and one weak HB) stands in direct contrast with the results of MD simulations, both with classical and *ab initio* potentials, which suggest instead that water would maintain the near tetrahedral local arrangement of ice (see table 4.1).

As already observed in section 2.4, such a discrepancy could be explained by the inability of classical force fields to reproduce all the subtle components of the HB interaction, particularly non–additive multi–body effects like cooperativity. *Ab-initio* MD simulations of water likely instead suffer from the incomplete representation of non–local effects such as van der Waals forces in the current DFT functionals as well as uncertainties in the description of angularly distorted HBs [51].

On the other hand it is evident, as shown in figure 4.6, that a liquid structure dominated by DD species, as proposed by MD simulations would generate XA spectra closer to that of bulk ice rather than presenting the sharp pre–edge and the intensity in the main–edge we expect from liquid water. The correct intensity distribution can instead be expected to result from spectra calculated for configurations with one donating and one accepting HB (fig. 4.6, D1A1), obtained by selecting from the CPMD trajectory structures that meet these criteria.

The resulting spectrum for this case does in fact show a better agreement with the experiment but fails to fully reproduce the sharp pre–edge of the liquid water spectrum at 535 eV. This finding places additional constraints, beyond the simple fulfillment of the "HB–cone" definition, on the possible local configurations

present in liquid water. This issue is further addressed in paper IV, where different geometrical criteria to select configurations from MD trajectories, which give XA spectra in agreement with experiment, are evaluated. The presence of a strong HB asymmetry, with one strong and one weak donating HB, seems to be necessary for the spectral signature of liquid water to develop.

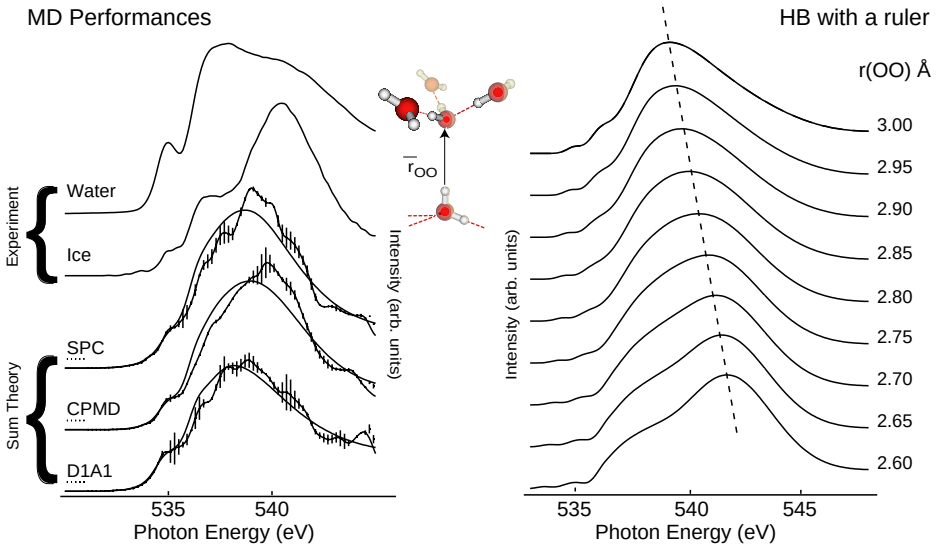

Figure 4.6: Sum spectra over typical HB configurations from a classical (SPC) MD and *ab initio* MD (CPMD) trajectory. Clusters composed of 32 molecules were used to obtain the simulated spectra. Only molecules with two HBs, one at the oxygen and one at the hydrogen side, were selected for the D1A1 sum spectrum. The discrete computed spectra were convoluted with constant 0.5 eV fwhm Gaussians and the error bars in the figures denote the standard deviation in the spectra (left). Simulated XAS for 17 water molecule clusters as function of the donating HB (oxygen–oxygen, **r**(OO)) distance (right).

Additionally to the pre–edge, valuable information on the HB network can be extracted, with the help of the theoretical analysis provided by DFT calculations, from the conduction band in the ice and liquid water spectra. The position of this band is in fact shown to be strongly dependent on the HB length, as summarized in figure 4.6.

The fact that the conduction band in the XA spectrum of water is broadened and presents intense features at both main- (537–538 eV) and post–edge (540–541 eV) region as compared to ice implies for the liquid a broader distribution of HB distance centered around a short ice–like (indicating saturated donating HB) and a longer value (weak donating HB), supporting the hypothesis of strongly asymmetrical HB configurations.

Finally, in paper VI we describe the implementation of the XAS calculation within the CPMD framework. The periodic conditions allow in principle a better description of the condensed phase, since the corresponding finite size effects, due to the artificial interaction of the core–hole with its periodic images, is a less severe

approximation than the neglect of long–range effects in the cluster model, which leads to the slow convergence of the XA spectra with increasing model size.

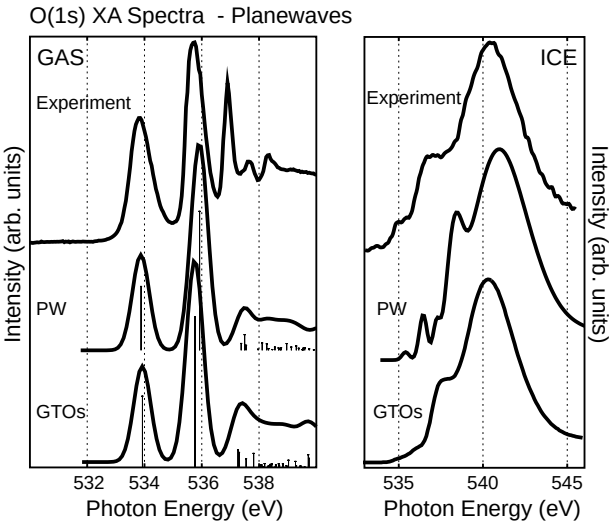

Figure 4.7: Calculated XA spectra for the gas phase H_2O using all–electron local basis (GTOs) and plane–waves (PW) methods, compared with experiment. Computed oscillator strengths are plotted with their respective convoluted spectra (left). Calculated XA spectra of ice with the cluster and the periodic PW approaches, compared with the experimental data (right). The periodic cell in the plane–waves calculation and the cluster for the all–electron calculations were composed of 64 and 44 molecules, respectively.

In the periodic plane–wave implementation the core–hole is introduced on the oxygen atom of interest through an *ad hoc* pseudopotential generated from an electronic–configuration $1s^{1.5}2s^22p^4$ with a fractional occupation of the 1s orbital. The spectrum calculation is performed without the reconstruction of the all–electron orbitals and, as such, the technique is applicable to all elements in the first row of the periodic table.

Most importantly, paper VI demonstrates the accuracy of the plane–wave approach in computing the XAS spectra by comparison with the results obtained with the all–electron cluster method. Figure 4.7 illustrates two cases of ice and gas phase water, which represent two well defined HB configurations.

However, particular care must be taken when comparing the generated spectra in the plane–wave pseudopotential approach with experiment because of the lack of an absolute energy scale in the computed spectra. As described in further detail in section 3.3.3, we overcome this difficulty by computing the necessary shift from all–electron calculations, while an arbitrary shift is otherwise used [122, 123]. In Ref. [122] this leads to the wrong interpretation of the XA spectrum of liquid water which is therein claimed to be well reproduced by the computed spectrum, using the FCH approximation, of a distribution of HB situations with only 19% broken donating HBs. However, when the absolute excitation energies are available and thus the theoretical spectra can be placed correctly against experiment, it

appears clear that neither the spectrum of bulk ice nor that of liquid water is well reproduced in the FCH approximation. As already mentioned in section 3.3.3 and demonstrated in further detail in paper VI, the HCH approximation, representing a better balance between initial and final state effects, is instead a more appropriate approach for the simulations of XA spectra of water in all its phases.

4.1.2 Excess Proton

The x–ray absorption spectrum of an acid solution also reveals some differences from that of bulk water. In particular, as depicted in figure 4.8, at high acid concentration the intensities at the pre- and main edge peaks (535-537 eV) decrease and the overall spectrum shifts to higher energies. Since XAS probes the distribution of instantaneous configurations in the solutions, these differences are expected to be due to the water molecules in closer interaction with the solvated proton or its counterion.

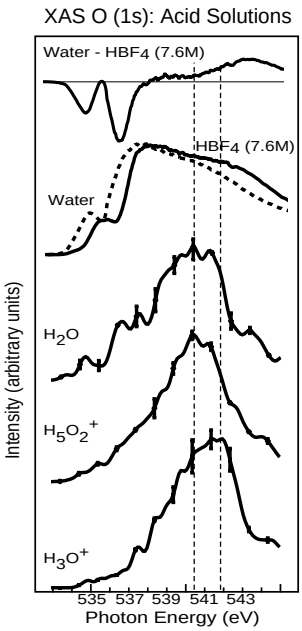

Figure 4.8: Experimental XAS spectra of a 7.6M HBF_4 solution (solid line), pure water (dashed line) and their difference spectra (top). Computed sum spectra for selected molecules in bulk water (H_2O), Eigen (H_3O^+) and Zundel ($H_5O_2^+$) configurations from an OSS2 molecular dynamics simulation. A constant Gaussian (0.5 eV fwhm) is used to convolute the original spectra. The vertical bars in the spectra indicate the standard deviations at a given energy in the set of selected molecules.

Comparison of the spectra of concentrated HCl and HBF_4 solutions shows that the change of anion does not affect the general shape of the spectra and thus the observed variations are a direct probe of the water molecule interacting with the excess proton.

In paper VII we use both model clusters of the optimized Eigen (H_3O^+) and Zundel ($H_5O_2^+$) proton forms and configurations extracted from a classical MD simulation of the excess proton in water (presented in fig. 4.8) for the theoretical analysis of the experimental spectra. From the simulated spectra it is possible to assign the increased intensity in the region above 541 eV to the presence of the H_3O^+ cation in water. The Zundel protonated cluster instead gives XA spectra which are similar in energy position and general appearance to that of liquid water. This is consistent with the fact that in the case of liquid water, the XA signal is only slightly sensitive to the HB coordination at the accepting side of the water molecule. The presence of the proton bridging two neighboring oxygen atoms in the $H_5O_2^+$ dimer thus does not strongly influence the spectrum, while the formation of a third intramolecular O–H bond is expected to have strong effects on the electronic structure of the water molecules.

Our results, consistent with the findings of a recent Monte Carlo simulation based on XRD data, suggest a preference of the excess proton for the Eigen (H_3O^+) form at low pH. This behavior of the highly concentrated solutions is maybe not unexpected, at least based on stoichiometric considerations (as the fraction of the excess proton increases there is less H_2O available to sustain polymeric forms of the protonated cation), yet our work provides the first spectroscopic evidence for a pH–dependent balance between the different species of protonated clusters.

4.1.3 Methanol

The sensitivity of the O–edge x–ray absorption spectroscopy to the HB environment, as observed for water, is confirmed in the case of methanol, discussed in paper VIII.

It is interesting to compare the development of the O K–edge spectrum of methanol (in fig. 4.9) upon HB formation with that of water. In water there are two equivalent H–donating possibilities, and with both coordinated the pre–edge feature is quenched, as discussed in depth previously. The pre–edge arises distinctly in the case of a strong (short) donating and one broken HB, of which the gas phase methanol represents an extreme example. In fact, in methanol the asymmetry is inherent through the strong covalent C–O bond compared with the O–H. Therefore, for methanol the pre–edge is quenched to a lesser extent through HB formation but is rather shifted to higher energies, since this bond cannot compete in strength with the internal C–O bond. DFT spectra calculations confirm that molecules with the O–H group saturated in a chain or ring exhibit a shift of ~ 1 eV of the pre–edge feature relative to the spectra of terminal uncoordinated molecules. This difference leads to a sequential shift of this feature with chain length that reflects the greater contribution of two hydrogen–bonded molecules in the interior of longer linear chains to the total n–mere spectrum. This behavior is summarized in figure 4.9.

With this in mind we can explain the changes between the experimental O K–edge spectra of surface and bulk methanol by concluding that a significant number of the molecules at the liquid surface occupy terminal positions and thus contribute to the intensity in the pre–edge region, while molecules donating an HB are dominant in the bulk, accounting for the shift in intensity from the pre–edge

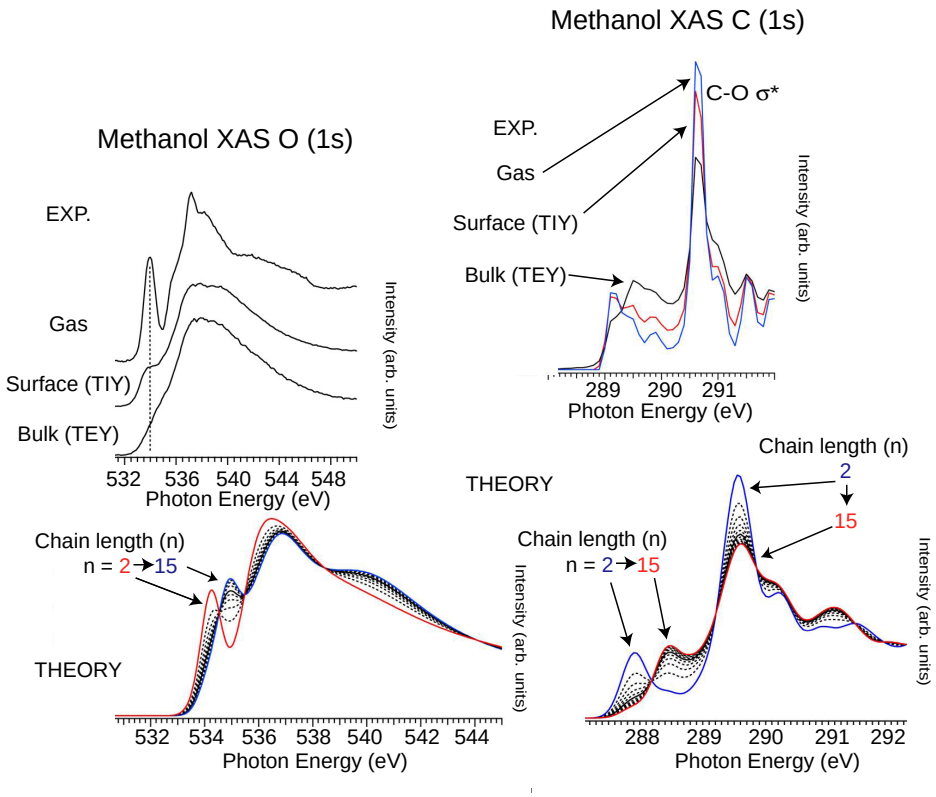

Figure 4.9: O (top, left) and C K–edge (top, right) experimental XAS spectra of a liquid methanol jet: gas phase, surface (TIY) and bulk (total electron yield, TEY). Composite spectra for O and C K–edge showing the evolution of oscillator strength with chain length, $(CH_3OH)_n$. Size range from n=2 to n=15 (bottom).

to the continuum band. This indicates a rearrangement of the hydrogen–bond topology from long chains and rings in the bulk liquid towards short linear chains (2–4 molecules in length) at the vacuum interface. As XA spectra are normally unaffected by the accepting HB environment, it is not possible to spectroscopically distinguish bifurcation from chains and rings and provide further validation for an equimolar mixture of eight–member linear chains and six–member rings in bulk methanol as proposed by a recent XES study [79].

Methanol molecules interact in the condensed phase through the HB interaction between the oxygen atoms leaving the local chemical environment of the methyl group (CH_3) unaffected[5], yet the C K–edge XA spectra of gas phase, surface and liquid bulk methanol, in figure 4.9, disclose a large degree of differences mirroring large changes in the electronic structure around the carbon atom caused by the HB

[5] A weak and short–lived interaction between the methyl group as HB donor and the oxygen of the nearest molecule as acceptor has been suggested from a recent *ab initio* MD simulation [77]. The models used for the spectra calculations in paper VIII do not account for this configuration.

interaction at the neighboring oxygen. Again, the progression from the monomer to long chains and rings is able to capture the gas–to–bulk shift of +0.5 eV and the systematic reduction of the C–O σ^* state observed by comparing the experimental vapor, surface and bulk spectra.

4.2 Electronic Structure

4.2.1 Transition Metal Ion–Water Interaction

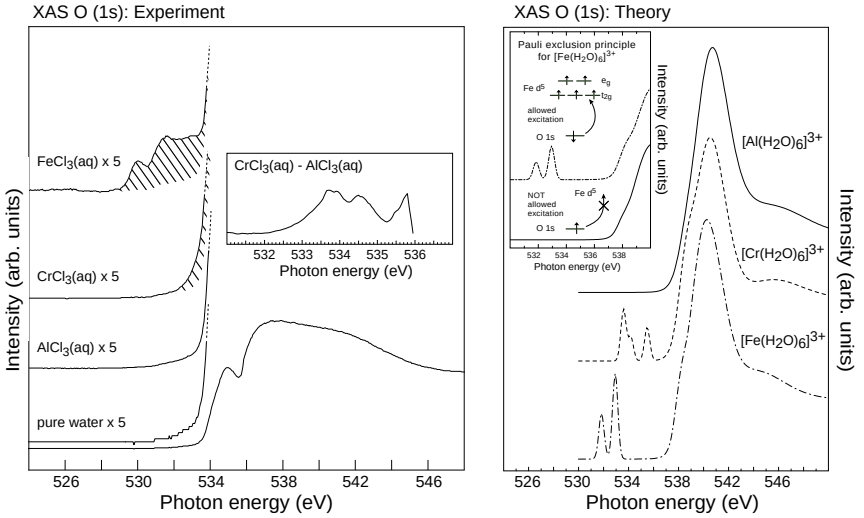

Figure 4.10: Experimental XAS spectra of pure water and Al^{3+}, Cr^{3+} and Fe^{3+} aqueous solutions. The shaded area indicates the pre–edge features assigned to the interaction of water with the d–orbital of the transition metals (left). In the inset these features are evident as differences between the Cr^{3+} and Al^{3+} aqueous solution spectra. Calculated spectra of a water molecule in $M(H_2O)_6{}^{3+}$ clusters, with M = Al, Cr, Fe (right). The computed spectra represent the sum of the contributions from excitation of a core–electron with parallel or antiparallel spin with respect to the electrons in the d–orbitals. The inset shows that, in the case of Fe^{3+} (aq), only electrons with antiparallel spins are allowed to interact with the d–orbitals.

The ability of XAS to act as a direct and local probe of the electronic structure around the excited atom is exemplified in the study of transition metal aqueous solutions carried out in paper IX. In this study we focus exclusively on the analysis of the low–energy region of the spectra, which yields information on the interaction between the solvated ion and the water molecules in its first hydration shell, and disregard the changes occurring in the continuum band, from which knowledge of the effects of solvation on the HB network of water can be extracted [152].

The experimental spectra of transition metal solutions, as shown in figure 4.10, are characterized by the presence in the pre–edge region (529–534 eV) of features of rather low intensity, with the exception of $FeCl_3$ (aq) where the signal is particularly enhanced, which are absent for liquid water and non d–ion solutions (e.g.

Al^{3+}).

Spectra calculations of small clusters, including the full first solvation shell of the cation, are able to reproduce these characteristic low–energy features in the transition metal ion solutions and their absence in the case of Al^{3+} (aq).

Since Al^{3+} and Cr^{3+} have very similar hydration spheres [153, 154] these features should be due mainly to differences in the electronic structure (i.e. the presence of open–shell d–orbitals in Cr^{3+}) and the nature of the interaction with the solvating water molecules. The Fe^{3+} ion represents an interesting test–case because in the small crystal field of water its high–spin state implies that the five outer electrons occupy all d–orbitals without pairing. In this way a core–electron with spin antiparallel to that of the five d–electrons can be excited into iron's d–orbitals, but this transition will be "Pauli forbidden" for electrons with parallel spin. Figure 4.10 presents a schematic view of this process. By computing XA spectra for excitations from both core spin–orbitals it is easy to prove that the low energy features indeed arise from orbitals centered around the oxygen atom which contain a certain degree of contribution from the d–orbital of the metal ion. In fact, only the computed spectrum of the spin–permitted excitation into the d–orbitals exhibits the characteristic peak of the experiment.

Furthermore, DFT calculations are able to demonstrate the great sensitivity displayed by XAS to the local environment of the solvated metal ion and that the formation of metal–chloride complexes that form in highly concentrated MCl solutions, can be fingerprinted by an upwards shift of the d–orbital–interaction–derived features.

4.2.2 The Hydrogen Bond

A hint on the origin of the changes that occur upon HB formation in the intensity of the pre–edge feature in the O (1s) spectra of water and methanol is provided by the comparison of the behavior of the corresponding a_1 state in the K–edge gas phase spectra of the isoelectronic hydrides CH_4, NH_3, H_2O and HF, given in figure 4.11. The a_1 lowest unoccupied molecular orbital (LUMO) in CH_4 contains only s–character, resulting from the tetrahedral symmetry of the molecule. Therefore methane manifests only negligible pre–edge intensity, arising from vibronic coupling to the asymmetric C–H bond stretching which breaks the symmetry. As the symmetry around the central atom is disrupted, like in ammonia and water, larger p–contributions appear in the a_1 state, resulting in the monotonically increasing spectral intensity in the pre–edge region which culminates in the giant line resonance for the linear HF molecule, whose a_1 LUMO orbital is almost entirely of p–character. Likewise, the absence of significant intensity in the pre–edge region in the XA spectrum of bulk ice can be related to the near–tetrahedral arrangement of protons around each O atom, which mimic the structure of CH_4. Conversely, upon deviation from the tetrahedral symmetry in liquid water caused by the breaking or weakening of hydrogen–bonds, it is expected to see similar changes in the XAS spectrum as between CH_4 and NH_3 with the increase of intensity of the pre–edge peak.

In paper X, using theoretical spectra simulations we are able to decompose the total XAS spectra of water molecules in different HB configurations into their p-

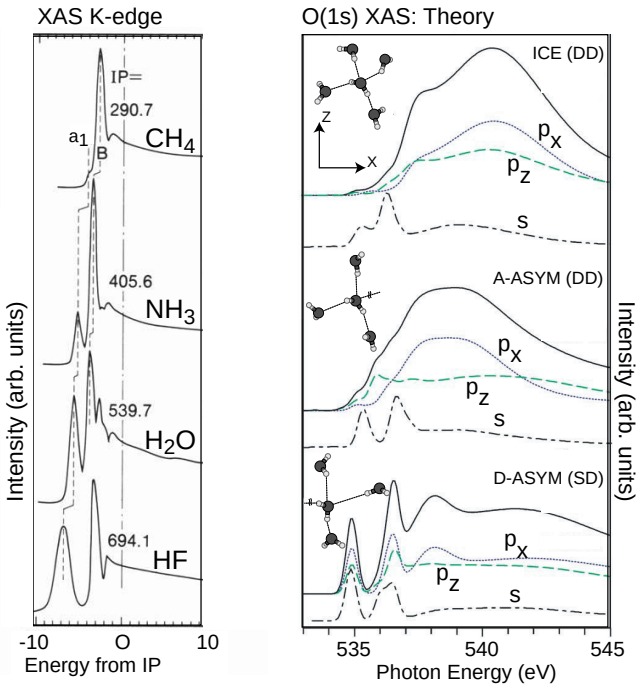

Figure 4.11: Experimental spectra of isoelectronic CH_4, NH_3, H_2O and HF from Ref. [81] (left). Computed XAS spectra for a broken donor (SD, D-ASYM) and acceptor (DD, A-ASYM) species in the liquid compared with that of Ice. Contributions from the p_x, p_z and s components are shown under their respective total spectrum (right).

and s–projections[6] and thus follow the nature of the s–p rehybridization of water's MOs in the different cases. In particular in ice the tetrahedral arrangement of the molecules causes an increase of the local symmetry resulting in orbitals of either pure 2s or 2p character (see figure 4.11).

On the other hand, breaking a donating HB provokes a disruption of the local symmetry and results in a s–p rehybridization of the water MOs which in turn allows significant p–contribution in the low–energy region of the XAS spectrum. The resulting antibonding orbital, localized along the O–H bond direction is mainly polarized towards the hydrogen atom[7] and thus particularly sensitive to the coordination of additional molecules at the donor rather than the HB acceptor side.

In paper XI we turn instead our attention to the changes in the occupied electronic structure of the water molecules upon HB formation, probed by PES

[6]The s–contribution, as described in section 3.3.2, is represented through the computed r^2 transition matrix elements. The p_z and p_x components give the O (2p) contributions to the $4a_1$ and $2b_1$ O–H antibonding orbital of the free H_2O molecule (axes defined in the insert of fig. 4.11). The p_y direction has been omitted in the graph since it lies in the direction of the $1b_2$ lone pair orbital and gives mainly contributions in the spectra from higher np shells.

[7]This behavior is expected since the corresponding bonding O–H orbital is polarized towards the oxygen, due to the difference in the electronegativity between the two atoms.

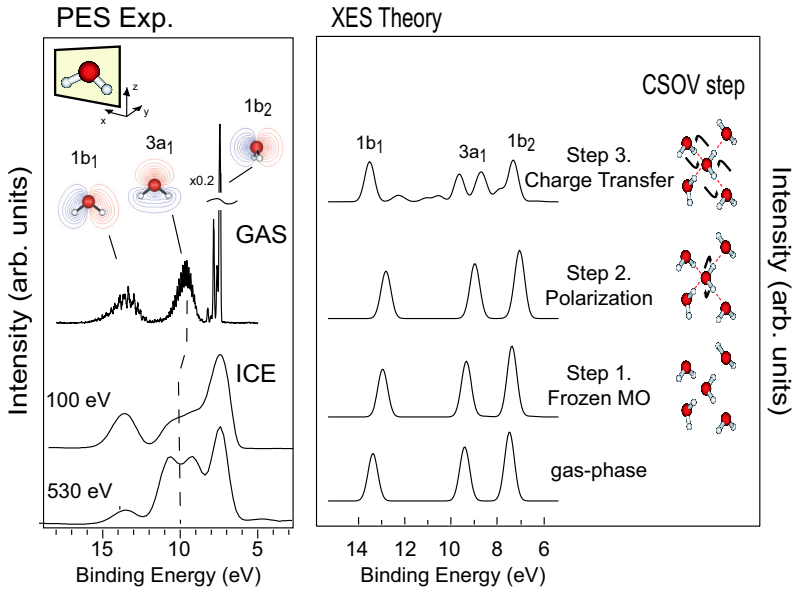

Figure 4.12: PES spectra of ice (left, bottom) and gas phase water (left, top). The calculated XE spectra corresponding to each step of the CSOV analysis of the tetrahedrally arranged H_2O pentamer cluster (right).

combined with DFT calculations. In the spectrum of the isolated H_2O the occupied $1b_1$, $3a_1$ and $1b_2$ orbitals are observed. Taking advantage of the strong dependence of the atomic photoionization cross–section on the incident photon energy, discussed in section 3.3.2, it is possible to enhance selectively the 2p or the 2s contributions in PES and thus obtain an experimental population analysis of the features composing the spectra. In figure 4.12 we observe that upon ice formation, the low–energy PES spectrum (yielding mainly 2p–contributions) presents a broader $1b_1$ peak and almost no intensity in the $3a_1$ feature compared to that of the gas phase. Conversely, the enhanced $3a_1$ in the high–energy PES reflects the s–character of this orbital.

By computing the charge occupation of the water MOs in ice and gas phase H_2O, it is observed that the lone–pair orbital $1b_2$ (fully occupied in the isolated molecule) looses part of its charge in ice and resulting in some b_2 character in the unoccupied space, giving a partial contribution in the p_y projection in the XAS spectrum. On the other hand the slight decrease in the s–population of the $3a_1$ orbital in the condensed phase can be interpreted as an indication of s–p rehybridization upon HB formation.

In paper XI we use the constrained space orbital variation (CSOV) analysis [29, 30] to investigate the contributions of the different orbital interactions to the binding energy and the XE spectra of a water molecule characterized by a full tetrahedral HB environment, as shown in figure 4.12.

In the CSOV analysis we perform a stepwise relaxation of the MOs in the pentamer cluster. Turning on coulomb and exchange repulsion (by bringing together, in step 1, the molecule in the pentamer geometry while retaining the gas phase MO

structure frozen) intramolecular (polarization, step 2) and intermolecular (charge transfer, step 3) orbital interactions one by one and following the effects on the occupied space of the central molecule by calculating the XES spectra. Full energetics of the HB is reached only after allowing intermolecular charge transfer which leads to s–p rehybridization. Moreover, only in the last step of the CSOV analysis, corresponding to the orbital mix between the two molecules, the computed spectrum undergoes changes in the $3a_1$ spectral region to match the experimental PES spectra. The reason why XES computed with the frozen ground state and dipole approximation can be used to reproduce the low–energy PES spectrum has already been discussed in section 3.1.2.

These results imply that a simple picture of the hydrogen–bond based on charge induction from the surrounding medium is able to reproduce neither the full energetics of the HB interaction nor the internal charge redistribution upon condensation, as probed by PES. Charge density difference (CDD) plots, discussed in detail in paper XI, demonstrate that the resulting effect of the observed charge redistribution is to minimize the Pauli repulsion, in order to allow for a stronger electrostatic interaction between the water molecules.

Chapter 5

Concluding Remarks

Now with five years of work finally condensed into these few pages it is probably only natural to ask ourselves, what is *really* water? How much more do we understand about it?

Certainly the interplay between local electronic structure measurements and theoretical analysis in this thesis has provided some more glimpse into the nature of this elusive substance; we have learned that the electronic structure of water changes dramatically when ice melts into the liquid, based on which we can hypothesize that the molecules form fewer but stronger HBs than previously imagined, that the HB interaction between water molecules involves a charge–transfer process and an extensive orbital rehybridization and that water binds to transition metal ions via the metal d–orbitals.

Yet the most important thing we have realized is that water, one oxygen and two hydrogen atoms linked in a kinked shape, is so evasive and complicated it cannot be described by more than 50 models, 70 parameters and a thousand research articles. If it is fair to say that no scientific project is ever really finished but only has good ending points[1], in the case of water there is no doubt that the research will be endless. Flexible, dynamic, complex and diverse, water seems to exist to challenge scientists to make continuous efforts to develop new experimental techniques and new theoretical tools.

As theoreticians we have no excuse for not doing so; the XAS measurements of liquid water stress the need to improve our modelling of the hydrogen–bond but at the same time provide a new set of data that complement previous information to guide us along the way.

Moreover, computer technology is advancing at an uncanny pace. Within this month alone that I have been writing this thesis, the title of most powerful supercomputer has changed owner twice with the current number one reaching the incredible peak performance of 65 Teraflops[2]. Only 20 years ago my Commodore 64, with its 8–bit processor and 64k of memory was the market killer, now all this seems like computer prehistory. Soon fantasy may be the only limit to the

[1] Like a PhD Thesis, for example.

[2] That's 65 thousand billions floating point operations per second.

development of new computational approaches and water and its anomalies will still be there to put them to the test.

Comments on my own participation

This work is the result of an extensive teamwork involving a lot of skillful people, to which I contributed playing an active role in the theoretical analysis, discussions and manuscript preparations. In particular, I'm responsible for the main part of the theoretical work in the papers which are included in this thesis, except paper I, to which I participated only at a later stage, paper III, where my contribution to the theoretical effort is limited to performing the CPMD simulations and the analysis of the MD trajectories, and paper XI in which I carried out the CSOV analysis and the corresponding spectrum calculations.

Acknowledgments

Lots of people helped me out with this. If I wouldn't have waited until the late hours of the last night to write this section maybe I could have found more appropriate words than those uttered below to sincerely thank all of them as much as they deserve.

I'm certainly much indebted to my supervisor Lars Pettersson for the guidance, helpfulness, encouragements and especially the infinite patience he put up with me during my PhD study, I hope this thesis is written to his reasonable satisfaction. I am also very thankful to Micheal Odelius and Anders Nilsson, without whose help and competence this would have been a much less valuable thesis.

I have learned a great deal of chemical physics (as well as innumerable other subjects) from endless conversations, ofter over extremely stretched coffee and lunch breaks, with Mats, Hirohito, Osamu, Lars–Åke, Nicole, Marcus, Arianna and the "Siegbahns", Oscar, Barbara, Fahmi and all other past and present members of the Quantum Chemistry groups at AlbaNova. I could not have hoped for a more supportive environment, I'll miss you very much. All coworkers are acknowledged. I'm grateful in particular to Philippe Wernet and Kevin Wilson for the fruitful collaborations and the discussions over coffee in California.

Lastly, it ought to be mentioned that this thesis could not have come into being without the help of Henrik Öström, who saved me a great deal of time with his LaTeX templates, Dennis Nordlund (I bet you recognize some of the figures of this thesis) and Theanne Schiros who voluntarily assumed the heavy duty of keeping me in a good mood and my thesis in a decent English. I cannot forget the artistic talent of my little(?) sister Anna, who helped out with the beautiful cover and the kindliness of Christina Schmitz, who spent one of her last Sunday afternoons in Stockholm taking scans of my brain so that I could have a picture of it in the introduction. Thank you all very much.

But it is to my friends and family who don't care about this thesis, who won't read this thesis but have been by my side during these last five years that this thesis is dedicated.

Matteo Cavalleri, Stockholm, November 2004

Crossword puzzle

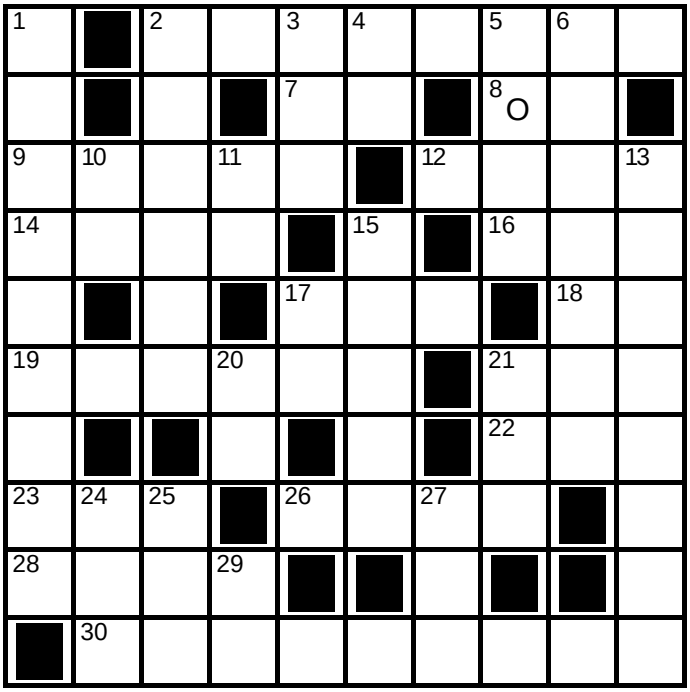

Across

2. Spanish City
7. Gold
8. Estonian Airlines (IATA code)
9. Spoken in Malaysia
12. Not this...
14. Bovine
16. Yoko...they say she ended the Beatles
17. Core-level spectroscopy
18. Hennes and Mauritz
19. Chemical element
21. Line, series
22. International Energy Agency
23. Above all
26. Town in northern italy
28. Lacking water
30. Swedish chemist, father of H_2O

Down

1. Juventus defender
2. Sport with a ball and a net
3. To cause to lie down
4. European Union
5. Small salmon
6. Walter Scott's disowned knight
10. Australia in the internet
11. Aluminium
13. Great American songwriter, whose "piano has been drinking"
15. Dance
17. X-ray emission
20. Germanium
21. City in Brazil
24. Sphere
25. Cake...American, giving an extra clue...
27. A unit of length equal to one thousandth of an inch, or 10 km if you speak Swedish
29. Title (that's related to this thesis)

Bibliography

[1] P. Ball, *H_2O. A biography of water* (Phoenix, London, 1999).

[2] Leonardo da Vinci, *Delle acque* (Sellerio Editore, Palermo, 2001).

[3] A.L. Lavoisier, Observations sur la physique **23**, 452 (1783).

[4] H.H. Meyer, Ann. d. Physik **5**, 701 (1930).

[5] G. W. Stewart, Phys. Rev. **37**, 9 (1931).

[6] E. Amaldi, Phys. Zeits. **32**, 914 (1931).

[7] R. Mecke, W. Baumann, and K. Freudenberg, Z. Physik **81**, 313, 445, 465 (1933).

[8] J.D. Bernal and R.H. Fowler, J. Chem. Phys. **1**, 515 (1933).

[9] L. Pauling, J. Am. Chem. Soc. **57**, 2680 (1935).

[10] J.A. Barker and R.O. Watts, Chem. Phys. Lett. **3**, 144 (1969).

[11] A. Rahman and F.H. Stillinger, J. Chem. Phys. **55**, 3336 (1971).

[12] B. Guillot, J. Molec. Liquids **101**, 219 (2002).

[13] K. Laasonen, M. Sprik, M. Parrinello, and R. Car, J. Chem. Phys. **99**, 9080 (1993).

[14] K. Muller-Dethlefs and P. Hobza, Chem. Rev. **100**, 143 (2000).

[15] S. Woutersen, U. Emmerichs, and H.J. Bakker, Science **278**, 658 (1997).

[16] L. Ojamäe and K. Hermansson, J. Phys. Chem. **98**, 4271 (1994).

[17] P.L. Silvestrelli and M. Parrinello, Phys. Rev. Lett. **82**, 3308 (1999).

[18] U.C. Singh and P. A. Kollman, J. Chem. Phys. **83**, 4033 (1985).

[19] L.X. Dang, J. Phys. Chem. B **102**, 620 (1998).

[20] P.-O. Åstrand, K. Ruud, K.V. Mikkelsen, and T. Helgaker, J. Phys. Chem. A **102**, 7686 (1998).

[21] J. Korchowiec and T. Uchimaru, J. Chem. Phys. **112**, 1623 (2000).

[22] A.E. Reed, L.A. Curtiss, and F. Weinhold, Chem. Rev. **88**, 899 (1988).

[23] S. Kashtanov, A. Augustsson, Y. Luo, J.-G. Guo, C. Såthe, J.-E. Rubensson, H. Siegbahn, J. Nordgren, and H. Ågren, Phys. Rev. B **69**, 024201 (2004).

[24] B. Barbiellini and A. Shukla, Phys. Rev. B **66**, 235101 (2002).

[25] E.D. Isaacs, A. Shukla, P.M. Platzman, D.R. Hamann, B. Barbiellini, and C.A. Tulk, Phys. Rev. Lett. **82**, 600 (1999).

[26] T.K. Ghanty, V.N. Staroverov, P.R. Koren, and E.R. Davidson, J. Am. Chem. Soc. **122**, 1210 (2000).

[27] E.D. Isaacs, A. Shukle, P.M. Platzman, D.R. Hamann, B. Barbiellini, and C.A. Tulk, Phys. Rev. Lett. **83**, 4445 (1999).

[28] P.L. Silvestrelli and M. Parrinello, J. Chem. Phys. **111**, 3572 (1999).

[29] P.S. Bagus, K. Hermann, and C.W. Bauschlicher Jr., J. Chem. Phys. **81**, 1966 (1984).

[30] P.S. Bagus, K. Hermann, and C.W. Bauschlicher Jr., J. Chem. Phys. **80**, 4378 (1984).

[31] A. Glebov, A.P. Graham, A. Menzel, J. P. Toennies, and P. Senet, J. Chem. Phys. **112**, 11011 (2000).

[32] N. Materer, U. Starke, A. Barbieri, M.A. Van Hove, and G.A. Somorjai, Surf. Sci. **381**, 190 (1997).

[33] J.P. Devlin, C. Joyce, and V. Buch, J. Phys. A **104**, 1974 (2000).

[34] L. Delzeit, J.P. Devlin, and V. Buch, J. Chem. Phys. **107**, 3726 (1997).

[35] D. Nordlund, H. Ogasawara, Ph. Wernet, M. Nyberg, M. Odelius, L.G.M. Pettersson, and A. Nilsson, Phys. Rev. Lett. submitted (2004).

[36] B. Rowland and J.P. Devlin, J. Chem. Phys. **94**, 812 (1991).

[37] X. Su, L. Lianos, Y.R. Shen, and G.A. Somorjai, Phys. Rev. Lett. **80**, 1533 (1998).

[38] H. Ogasawara, N. Horimoto, and M. Kawai, J. Chem. Phys. **112**, 8229 (2000).

[39] R. Romberg, S.P. Frigo, A. Ogurtsov, P. Feulner, and D. Menzel, Surf. Sci. **451**, 116 (2000).

[40] Ph. Parent, C. Laffon, C. Mangeney, F. Bournel, and M. Tronc, J. Chem. Phys. **117**, 10842 (2002).

[41] C.J. Fecko, J.D. Eaves, J.J. Loparo, A. Tokmakoff, and P.L. Geissler, Science **301**, 1698 (2003).

[42] R. Ludwig, Angew. Chem. Int. Ed. **40**, 1808 (2001).

[43] T. Head-Gordon and G. Hura, Chem. Rev. **102**, 2651 (2002).

[44] A.K. Soper, Chem. Phys. **258**, 121 (2000).

[45] B. Tomberli, C.J. Benmore, P.A. Egelstaff, J. Neuefeind, and V. Honkimäki, J. Phys. Cond. Matt. **12**, 2597 (2000).

[46] J.H. Root, P.A. Egelstaff, and A. Hime, Chem. Phys. **109**, 5164 (1986).

[47] B. Guillot and Y. Guissani, J. Phys. Chem. **108**, 10162 (1998).

[48] J. Lobaugh and G.A. Voth, J. Chem. Phys. **106**, 2400 (1997).

[49] K. Modig, B.G. Pfrommer, and B. Halle, Phys. Rev. Lett. **90**, 075502 (2003).

[50] J. Stenger, D. Madsen, P. Hamm, E.T.J. Nibbering, and T. Elsaesser, Phys. Rev. Lett. **87**, 027401 (2001).

[51] J. Ireta, J. Neugebauer, and M. Scheffler, J. Phys. Chem. A **108**, 5692 (2004).

[52] Q. Du, R. Superfine, E. Freysz, and Y.R. Shen, Phys. Rev. Lett. **70**, 2313 (1993).

[53] K.R. Wilson, B.S. Rude, T. Catalano, R.D. Schaller, J.G. Tobin, D. T. Co, and R.J. Saykally, J. Phys. Chem. B **105**, 3346 (2001).

[54] I.-F. W. Kuo and C.J. Mundy, Science **303**, 658 (2004).

[55] F. Franks, *Water - A comprehensive treatise* (Plenum Press, New York–London, 1972), Vol. I.

[56] A.W. Omta, M.F. Kropman, S. Woutersen, and H.J. Bakker, Science **301**, 347 (2003).

[57] H. Ohtaki and T. Rodai, Chem. Rev. **93**, 1157 (1993).

[58] T. Yamaguchi, M. Niihara, T. Takamaku, H. Wakita, and H. Kanno, Chem. Phys. Lett. **274**, 485 (1997).

[59] J.C. Hindman, A. Svirmickas, and M. Wood, J. Phys. Chem. **59**, 1517 (1974).

[60] R.D. Davy and M.B. Hall, Inorg. Chem. **27**, 1417 (1988).

[61] M. Eigen, Angew. Chem. Int. Ed. **3**, 1 (1964).

[62] G. Zundel and H. Metzer, Z. Phys. Chem. **58**, 225 (1968).

[63] F.S. Lee and G.B. Carpenter, J. Phys. Chem. **63**, 279 (1959).

[64] R.E. Richards and J.A.S. Smith, Trans. Faraday Soc **47**, 1261 (1951).

[65] Y. Kakiuchi, H. Shono, H. Komatsu, and K. Kigoshi, J. Chem. Phys. **19**, 1069 (1951).

[66] D.E. Bethell and N. Sheppard, J. Chem. Phys. **21**, 1421 (1953).

[67] R.C. Taylor and G.L. Vidale, J. Am. Chem. Soc. **78**, 5999 (1956).

[68] M.E. Tuckerman, K. Laasonen, M. Sprik, and M. Parrinello, J. Phys. Chem. **99**, 5749 (1995).

[69] M.E. Tuckerman, K. Laasonen, M. Sprik, and M. Parrinello, J. Chem. Phys. **103**, 150 (1995).

[70] D. Marx, M.E. Tuckerman, J. Hutter, and M. Parrinello, Nature **397**, 601 (1999).

[71] A. Botti, F. Bruni, S. Imberti, M.A. Ricci, and A.K. Soper, J. Chem. Phys. **121**, 7840 (2004).

[72] N. Agmon, J. Phys. Chem. A **102**, 192 (1998).

[73] S. Sarkar and R.N. Joarder, J. Chem. Phys. **99**, 2032 (1993).

[74] T. Yamaguchi, K. Hidaka, and A.K. Soper, Mol. Phys. **96**, 1159 (1999).

[75] T. Yamaguchi, K. Hidaka, and A.K. Soper, Mol. Phys. **97**, 603 (1999).

[76] L. Pauling, *The nature of the chemical bond* (Cornell University, Ithaca, NY, 1960).

[77] M. Pagliai, G. Cardini, R. Righini, and V. Schettino, J. Chem. Phys. **119**, 6655 (2003).

[78] Y. Tanaka, N. Ohtomo, and H. Arakawa, Bull. Chem. Soc. Jpn. **58**, 270 (1985).

[79] J.-H. Guo, Y. Luo, a. Augustsson, S. Kashtanov, J.-E. Rubensson, D.K. Shuh, H. Ågren, and J. Nordgren, Phys. Rev. Lett. **91**, 157401 (2003).

[80] K.R. Wilson, R.D. Schaller, D.T. Co, R.J. Saykally, B.S. Rude, T. Catalano, and J.D. Bozek, J. Chem. Phys. **117**, 7738 (2002).

[81] J. Stöhr, *NEXAFS spectroscopy* (Springer-Verlag, Berlin, 1992).

[82] A. Nilsson and L.G.M. Pettersson, Surf. Sci. Reports **55**, 49 (2004).

[83] J. Stöhr, F. Sette, and A.L. Johnson, Phys. Rev. Lett. **53**, 1684 (1984).

[84] A. Bianconi, Appl. Surf. Sci. **6**, 392 (1980).

[85] Y. Mizuno and Y. Ohmura, J. Phys. Soc. Jpn. **22**, 445 (1967).

[86] T. Suzuki, J. Phys. Soc. Jpn. **22**, 1139 (1967).

[87] M. T. Seiger, W.C. Simpson, and T.M. Orlando, Phys. Rev. B **56**, 4925 (1997).

[88] D. Coulman, A. Puschmann, U. Höfer, H.-P. Steinrück, W. Wurth, P. Feulner, and D. Menzel, J. Chem. Phys. **93**, 58 (1990).

[89] B. Brena, D. Nordlund, M. Odelius, H. Ogasawara, A. Nilsson, and L.G.M. Pettersson, Phys. Rev. Lett. **93**, 148302 (2004).

[90] S. Hüffner, *Photoelectron Spectroscopy*, *Springer Ser. Sol. Stat. Sci.* (Springer-Verlag, Berlin, 1996).

[91] P.E.M. Siegbahn, Quar. Rev. Biophys. **36**, 91 (2003).

[92] M.R.A. Blomberg and P.E.M. Siegbahn, J. Phys. Chem. B **105**, 9375 (2001).

[93] F. Himo and P.E.M. Siegbahn, Chem. Rev. **103**, 2421 (2003).

[94] Z. Lodziana, N.-Y. Topsøe, and J.K. Nørskov, Nature Mat. **3**, 289 (2004).

[95] A. Szabo and N.S. Ostlund, *Modern Quantum Chemistry*, 2nd ed. (McGraw–Hill, New York, 1989).

[96] M. Born and R. Oppenheimer, Ann. d. Physik **84**, 457 (1927).

[97] D.R. Hartree, Proc. Cam. Phil. Soc. **24**, 89 (1928).

[98] V. Fock, Z. Physik **61**, 209 (1930).

[99] R.J. Bartlett and J. Stanton, in *Reviews in computational chemistry*, edited by K.B. Lipkowitz and Boyd D.B. (VCH Publishers, New York, 1994), Vol. V.

[100] R.G. Parr and W. Yang, *Density-functional theory of atoms and molecules* (Oxford Univ Press, Oxford, 1989).

[101] N.C. Handy, in *European summerschool in quantum chemistry*, edited by B.O. Roos and P.-O. Widmark (Lund University, Lund, 2000), Vol. II, Chap. X, pp. 505–548.

[102] J.K. Labanowski and J.W. Andzelm, *Density functional methods in chemistry* (Springer–Verlag, New York, 1991).

[103] H. Thomas, Proc. Cam. Phil. Soc. **23**, 542 (1927).

[104] E. Fermi, Acc. Naz. Lincei **6**, 602 (1927).

[105] P. Hohenberg and W. Kohn, Phys. Rev. **136**, B864 (1964).

[106] W. Kohn and L.J. Sham, Phys. Rev. **140**, A1133 (1965).

[107] J.C. Slater, Phys. Rev. **81**, 385 (1951).

[108] S. Kurth, J.P. Perdew, and P. Blaha, Int. J. Quant. Chem. **75**, 889 (1999).

[109] A.D. Becke, Phys. Rev. A **38**, 3098 (1988).

[110] J.P. Perdew and Y. Wang, Phys. Rev. B **33**, 8800 (1986).

[111] C. Lee, W. Yang, and R.G. Parr, Phys. Rev. B **37**, 785 (1988).

[112] A.D. Becke, J. Chem. Phys. **98**, 5648 (1993).

[113] Y. Andersson, D.C. Langreth, and B.I. Lundqvist, Phys. Rev. Lett. **76**, 102 (1996).

[114] M. Kamiya, T. Tsuneda, and Hirao K., J. Chem. Phys. **117**, 6010 (2002).

[115] M. Dion, H. Rydberg, E. Schröder, D.C. Langreth, and B.I. Lundqvist, Phys. Rev. Lett. **92**, 246401 (2004).

[116] H. Ågren, V. Carravetta, O. Vahtras, and L. G. M. Pettersson, Chem. Phys. Lett. **222**, 75 (1994).

[117] A. Nilsson and N. Mårtensson, Physica B **208&209**, 19 (1995).

[118] U. von Barth and G. Grossmann, Phys. Rev. B **25**, 5150 (1982).

[119] V. I. Grebennikov, Y. A. Babanov, and O. B. Sokolov, Phys. Stat. Sol. **79**, 1773 (1977).

[120] L. Triguero, L.G.M. Pettersson, and H. Ågren, Phys. Rev. B **58**, 8097 (1998).

[121] I. Tanaka, H. Araki, M. Yoshiya, T. Mizoguchi, K. Ogasawara, and H. Adachi, Phys. Rev. B **60**, 4944 (1999).

[122] B. Hetényi, F. De Angelis, P. Gianozzi, and R. Car, J. Chem. Phys. **120**, 8632 (2004).

[123] M. Taillefumier, D. Cabaret, A.-M. Flank, and F. Mauri, Phys. Rev. B **66**, 195107 (2002).

[124] J.C. Slater, Adv. Quant. Chem. **6**, 1 (1972).

[125] J.C. Slater and K.H. Johnsson, Phys. Rev. B **5**, 844 (1972).

[126] C. Kolczewski, R. Püttner, O. Plashkevych, H. Ågren, V. Staemmler, M. Martins, G. Snell, A.S. Schlachter, M. Sant'Anna, G. Kaindl, and L. G. M. Pettersson, J. Chem. Phys. **115**, 6426 (2001).

[127] M. Nyberg, M. Odelius, A. Nilsson, and L. G. M. Pettersson, J. Chem. Phys. **119**, 12577 (2003).

[128] H. Öström, L. Triguero, K. Weiss, H. Ogasawara, M.G. Garnier, D. Nordlund, M. Nyberg, L. G. M. Pettersson, and A. Nilsson, J. Chem. Phys. **118**, 3782 (2003).

[129] M. Nyberg, Y. Luo, L. Triguero, L. G. M. Pettersson, and H. Ågren, Phys. Rev. B **60**, 7956 (1999).

[130] L. Triguero, O. Plashkevych, L. G. M. Pettersson, and H. Ågren, J. Electron Spectrosc. Relat. Phenom. **104**, 215 (1999).

[131] A. Föhlisch, J. Hasselström, P. Bennich, N. Wassdahl, O. Karis, A. Nilsson, L. Triguero, M. Nyberg, and L.G.M. Pettersson, Phys. Rev. B **61**, 16229 (2000).

[132] L. Triguero, L.G.M. Pettersson, and H. Ågren, J. Phys. Chem. **102**, 10599 (1998).

[133] J.J. Yeh and I. Lindau, Atom. Data Nucl. Data **32**, 1 (1985).

[134] K. Hermann, L.G.M. Pettersson, M.E. Casida, C. Daul, A. Goursot, A. Koester, E. Proynov, A. St-Amant, D.R. Salahub (Contributing Authors) V. Carravetta, H. Duarte, N. Godbout, J. Guan, C. Jamorski, M. Leboeuf, V. Malkin, O. Malkina, M. Nyberg, L. Pedocchi, F. Sim, L. Triguero, and A. Vela, StoBe-deMon version 2.0, StoBe Software, 2002.

[135] W. Kutzelnigg, U. Fleischer, and M. Schindler, *NMR-Basic Principles and Progress* (Springer-Verlag, Heidelberg, 1990).

[136] L. G. M. Pettersson, U. Wahlgren, and O. Gropen, J. Chem. Phys. **86**, 2176 (1987).

[137] M. Nyberg, Ph.D. thesis, Stockholm University, 2000.

[138] H. Ågren, V. Carravetta, O. Vahtras, and L. G. M. Pettersson, Theo. Chem. Acc. **97**, 14 (1997).

[139] CPMD V3.7, Copyright IBM Corp 1990-2004, Copyright MPI fuer Festkoerperforschung Stuttgart 1997-2001.

[140] H. Öström, L. Triguero, M. Nyberg, H. Ogasawara, L.G.M. Pettersson, and A. Nilsson, Phys. Rev. Lett. **91**, 046102 (2003).

[141] A. Föhlisch, M. Nyberg, P. Bennich, L. Triguero, J. Hasselström, O. Karis, L.G.M. Pettersson, and A. Nilsson, J. Chem. Phys. **112**, 1946 (2000).

[142] A. Föhlisch, M. Nyberg, J. Hasselström, O.Karis, L.G.M. Pettersson, and A. Nilsson, Phys. Rev. Lett. **85**, 3309 (2000).

[143] L. Triguero and L.G.M. Pettersson, Surf. Sci. **398**, 70 (1998).

[144] L. Triguero, Y. Luo, L.G.M Pettersson, H. Ågren, P. Väterlein, M. Weinelt, A. Föhlish, J. Hasselström, O. Karis, and A. Nilsson, Phys. Rev. B **59**, 5189 (1999).

[145] L. Triguero, A. Föhlish, P. Väterlein, J. Hasselström, M. Weinelt, L.G.M. Pettersson, Y. Luo, H. Ågren, and A. Nilsson, J. Am. Chem. Soc. **122**, 12310 (2000).

[146] O. Takahashi and L. G. M. Pettersson, J. Chem. Phys. in press (2004).

[147] D. T. Bowron, M. H. Krisch, A. C. Barnes, J. L. Finney, A. Kaprolat, and M. Lorenzen, Phys. Rev. B **62**, R9223 (2000).

[148] L. Ojamäe, I. Shavitt, and S. Singer, J. Chem. Phys. **109**, 5547 (1998).

[149] G.C. Lie and E. Clementi, Phys. Rev. A **33**, 2679 (1986).

[150] K. Toukan and A. Rahman, Phys. Rev. B **31**, 2643 (1985).

[151] F. Weinhold, J. Chem. Phys. **109**, 373 (1998).

[152] L.Å. Näslund, D.C. Edwards, U. Bergmann, Ph. Wernet, H. Ogasawara, L.G.M. Pettersson, S. Myneni, and A. Nilsson, in manuscript (2004).

[153] L. Helm and A.E. Merbach, Coor. Chem. Rev. **187**, 15 (1999).

[154] J.K. Beattie, S.P. Best, B.W. Skelton, and A.H. White, J. Chem. Soc., Dalton Trans. **1981**, 2105 (1981).